



Akkermansia muciniphila exacerbates food allergy in fibre-deprived mice

Received: 10 June 2022

Accepted: 5 August 2023

Published online: 11 September 2023

Amy Parrish^{1,2,5}, Marie Boudaud^{1,6}, Erica T. Grant^{1,2}, Stéphanie Willieme¹, Mareike Neumann^{1,2}, Mathis Wolter^{1,2}, Sophie Z. Craig^{1,2}, Alessandro De Sciscio¹, Antonio Cosma^{1,3}, Oliver Hunewald¹, Markus Ollert^{1,4} & Mahesh S. Desai^{1,4}

Check for updates

Alterations in the gut microbiome, including diet-driven changes, are linked to the rising prevalence of food allergy. However, little is known about how specific gut bacteria trigger the breakdown of oral tolerance. Here we show that depriving specific-pathogen-free mice of dietary fibre leads to a gut microbiota signature with increases in the mucin-degrading bacterium *Akkermansia muciniphila*. This signature is associated with intestinal barrier dysfunction, increased expression of type 1 and 2 cytokines and IgE-coated commensals in the colon, which result in an exacerbated allergic reaction to food allergens, ovalbumin and peanut. To demonstrate the causal role of *A. muciniphila*, we employed a tractable synthetic human gut microbiota in gnotobiotic mice. The presence of *A. muciniphila* within the microbiota, combined with fibre deprivation, resulted in stronger anti-commensal IgE coating and innate type-2 immune responses, which worsened symptoms of food allergy. Our study provides important insights into how gut microbes can regulate immune pathways of food allergy in a diet-dependent manner.

As the Western world continues to see rising rates of food allergy^{1,2} that cannot be explained solely by genetics^{3,4}, identifying mechanisms of sensitization that are driven by environmental factors has become increasingly important. The gut microbiota has been shown to play an important role in food allergy by inducing protection against sensitization^{5–7}. This is evident from studies in germ-free (GF) mice that develop severe anaphylaxis, which can be dampened with the colonization of single microbes or complex communities of bacteria⁷. Moreover, mouse studies utilizing high-fat⁸ or low-fibre⁹ diets have shown that diet-mediated changes in the gut microbiota are associated with food allergy sensitization. Nevertheless, little is known about the causal links between food allergy sensitization and specific members of the microbiome, and how certain microbes regulate allergic responses.

Sensitization in atopic diseases begins at barrier sites and, in the context of food allergy, a functional epithelial barrier has been shown to be crucial in preventing sensitization and promoting oral tolerance³.

An important part of the intestinal mucosal barrier is the mucus layer, which serves as a first line of defence in the gut to prevent microbial invasion but allow nutrient absorption^{10,11}. Although gut exposure to allergens is understood to induce immunotolerance in a healthy gut, tolerance breakdown may occur when the mucus layer is genetically ablated, as shown in *Muc2*^{-/-} mice that lack the gene for *O*-glycosylated mucin-2 (MUC2), the main constituent of the mucus layer¹². Induction of tolerance in the gut through regulatory T cells is mediated by the sensing of MUC2 by local dendritic cells (DC), highlighting the importance of the mucus barrier in food allergy^{12,13}.

Diet is an important environmental factor that affects the mucus barrier through the microbiota because: (1) dietary fibre deprivation increases deterioration of the colonic mucus layer by mucolytic gut bacteria^{14,15}, and (2) Western-style diet increases the permeability of the colonic mucus layer¹⁶. Fibre-deprived microbiota-mediated mucus barrier dysfunction is reflected in enhanced susceptibility to infection

¹Department of Infection and Immunity, Luxembourg Institute of Health, Esch-sur-Alzette, Luxembourg. ²Faculty of Science, Technology and Medicine, University of Luxembourg, Esch-sur-Alzette, Luxembourg. ³National Cytometry Platform, Luxembourg Institute of Health, Esch-sur-Alzette, Luxembourg.

⁴Odense Research Center for Anaphylaxis, Department of Dermatology and Allergy Center, Odense University Hospital, University of Southern Denmark, Odense, Denmark. ⁵These authors contributed equally: Amy Parrish, Marie Boudaud. e-mail: mahesh.desai@lih.lu

by *Citrobacter rodentium*, a pathogen that must cross the mucus layer to reach the gut epithelium and initiate mucosal infection^{14,17}. Nevertheless, little is known about how diet-mediated barrier dysfunction together with increased activities of specific mucin-degrading microbes might impact oral tolerance.

In this Article, we hypothesized that dietary fibre deprivation, which can drive a mixed type 1 and 2 immune landscape together with an increase in mucin-degrading gut microbes, predisposes the host to enhanced allergen sensitization. Using two experimental allergens, ovalbumin and peanut, we establish a causal link between *Akkermansia muciniphila* and allergic immune responses by promoting type-2 immunity.

Results

Fibre deprivation leads to microbiota-mediated colonic barrier dysfunction

We fed specific-pathogen-free (SPF) BALB/c mice for 40 days on a fibre-rich (FR) (standard laboratory chow) or a fibre-free (FF) diet. In line with our previously published results in gnotobiotic mice with a characterized 14-member synthetic human gut microbiota (14SM)¹⁴, the microbiota of FF-fed mice exhibited increased relative abundances of bacteria belonging to the known mucin-specialist genus *Akkermansia* (Fig. 1a). In addition, other putative mucin-degrading species (Fig. 1a, shown in bold), such as *Mucispirillum*¹⁸ and *Parabacteroides*¹⁹, were also increased in the FF-fed mice.

In line with previous findings^{14,15,17}, the FF-fed mice exhibited approximately 2-fold reduction in colonic mucus thickness (Fig. 1b,c and Extended Data Fig. 1a,b). Using an ex vivo ex situ method to assess the penetrability of the mucus on dissected colonic tissues²⁰, we found that the mucus displayed similar normalized penetrability to bacteria-sized fluorescent beads between the two diets (Fig. 1d and Extended Data Fig. 1c,d). Intriguingly, with this method, the overall mucus thickness, determined as the distance of the beads from the epithelium was significantly higher in the FF-fed mice, suggesting changes in mucus architecture under fibre deprivation (Extended Data Fig. 1c–e). Fibre deprivation did not affect the number of goblet cells per crypt (Fig. 1e), suggesting that mucus production is not affected by diet. However, despite a similar penetrability of the colonic mucus to bacteria-sized beads (Fig. 1d), the overall intestinal permeability to FITC-dextran was increased in FF-fed mice (Fig. 1f), suggesting a higher permeability of the overall gut mucosal barrier to luminal antigens during fibre deprivation.

The relative transcript levels of the epithelial-derived cytokines²¹, IL-25, IL-33 and TSLP, were increased in the colon and/or in the caecum, but not in the ileum, in FF-fed mice (Fig. 1g,h and Extended Data Fig. 1f). Consistently, the *Il5* transcript tended to be increased in FF caecal tissues (Extended Data Fig. 1f). In addition, FF-fed mice displayed increased levels of type 1 and 17 cytokine transcripts, *Ifng*, *Tnfa*, *Il22* and *Il17a* in the colon (Fig. 1i,j and Extended Data Fig. 1f). Although the higher transcriptional levels of inflammatory cytokines were not reflected in the faecal level of the neutrophilic inflammatory marker lipocalin (LCN-2) (Extended Data Fig. 1g), these data reveal an inflammatory response reflective of a gut barrier impairment that is specific to the lower intestinal tract (caecum and colon) under fibre deprivation. Intriguingly, tissues from fibre-deprived GF mice seemed to have slightly higher levels of *Il25* and *Il33* in the colon compared with FR tissues, while *Tslp* expression was barely detectable and, *Ifng* and *Tnfa* remained at low levels compared with those from SPF FF-fed mice (Extended Data Fig. 1h), suggesting that FF diet alone in the absence of microbiota contributes to some of the immune changes.

Colonic barrier dysfunction is associated with local type-2 inflammation

Using mass cytometry by time-of-flight (CyTOF)-based broad immunophenotyping, our recently prepublished data showed that

FF-fed mice exhibit a biased immune landscape in the colonic lamina propria (cLP), with an increase in type-2 inflammatory cells such as ILC2, mast cells and activated Th2 cells²². Targeted fluorescence-activated cell sorting (FACS) analysis revealed a higher frequency of eosinophils in the colon and ileum of FF-fed mice (Fig. 2a, two-way analysis of variance (ANOVA), diet effect $P = 0.0281$; and Extended Data Fig. 2a), along with a higher frequency of IL-5-producing CD4⁺ and/or CD8⁺ T cells in the colon and ileum (Fig. 2b–e and Extended Data Fig. 2b). Consistent with an overall increase in activated CD69⁺ T cells²², FF-fed mice had also more IFNy-, IL-13- and IL-17-producing T cells in the colon (Fig. 2b,c), while in the ileum, only IFNy-producing T cells were enriched in addition to IL-5-producing cells (Fig. 2d,e). The titres of serum IgE and IgG1 were not different between the two dietary groups, although they were higher in SPF than in GF mice (Fig. 2f and Extended Data Fig. 2c). However, the titres of mast cell protease 1 (MCPT1) were reduced in the FF-fed SPF mice compared with FR-fed SPF mice, but not in the GF control groups (Extended Data Fig. 2c). On the basis of the serum data, these results show that FF-fed mice develop a type-2 immune profile that is restricted to the gut.

To determine whether the increased type-2 inflammation within the colon could be reflected in the anti-commensal antibody response, we analysed the IgA- and IgE coating of faecal bacteria over the 40-day feeding period. As expected, bacteria were mainly coated with IgA, with a detection of ~30% IgA-coated bacteria at the beginning of the timecourse and remaining relatively stable between the two diets over time (Fig. 2g). In contrast, IgE-coated bacteria were almost undetectable at the beginning of the experiment and increased over time in FF-fed mice only, reaching up to 2% of faecal bacteria at week 5 (Fig. 2h and Extended Data Fig. 2d). In contrast, ileal bacteria remained minimally coated with IgE in both groups (Fig. 2i). In line with the barrier breakdown profiles (Fig. 1), these results: (1) support a colon-specific, anti-commensal IgE response driven by FF diet; and (2) point to a possible mechanism of allergic sensitization through a more permeable intestinal barrier and a type-2 skewed immune landscape.

Diet-driven barrier dysfunction is reflected in exacerbated food allergic responses

We further hypothesized that the FF-fed mice may be rendered more susceptible to food allergen sensitization via the oral route. To test this hypothesis, mice were sensitized with ovalbumin (OVA) via the gastro-intestinal route by gavaging the allergen along with cholera toxin (CTX) as an adjuvant to promote the breakdown of oral tolerance and induce allergic reactions with moderate severity as previously described (Fig. 3a)²³. The FF diet or sensitization did not affect the weight gain of mice over time (Extended Data Fig. 3). Upon allergen challenge, FF-fed sensitized (OVA-CTX) mice exhibited more severe anaphylactic symptom scores (Fig. 3b) and a greater drop in core body temperature (Fig. 3c) compared with FR-fed sensitized (OVA-CTX) mice. Interestingly, FF-fed mice that were exposed solely to the allergen without adjuvant (OVA) or with PBS only also exhibited slightly increased symptom scores compared with their FR-fed controls, suggesting an effect of fibre deprivation on mild allergen-independent symptoms (Fig. 3b). Nevertheless, OVA-specific IgE and IgG1 were detectable only in the serum of OVA-CTX mice, confirming the model of adjuvant-mediated breakdown of oral tolerance²³ (Fig. 3d). Fibre deprivation did not affect the level of sensitization as defined by the serum titres of OVA-specific IgE and IgG1 (Fig. 3d). Sensitization did not increase the overall frequency of IgE-coated bacteria (Fig. 3e) compared to FF-fed unsensitized mice (Fig. 2i), signifying that the increased IgE coating occurs independently of allergen sensitization. In addition, our data show an increase in total IgE and IgG1 in OVA-CTX-sensitized mice compared with unsensitized mice, and higher total IgE in FF-fed mice compared with FR-fed mice regardless of treatment (Fig. 3f). Of note, while the total IgE titres did not differ between FR- and FF-fed mice after 40 d of feeding

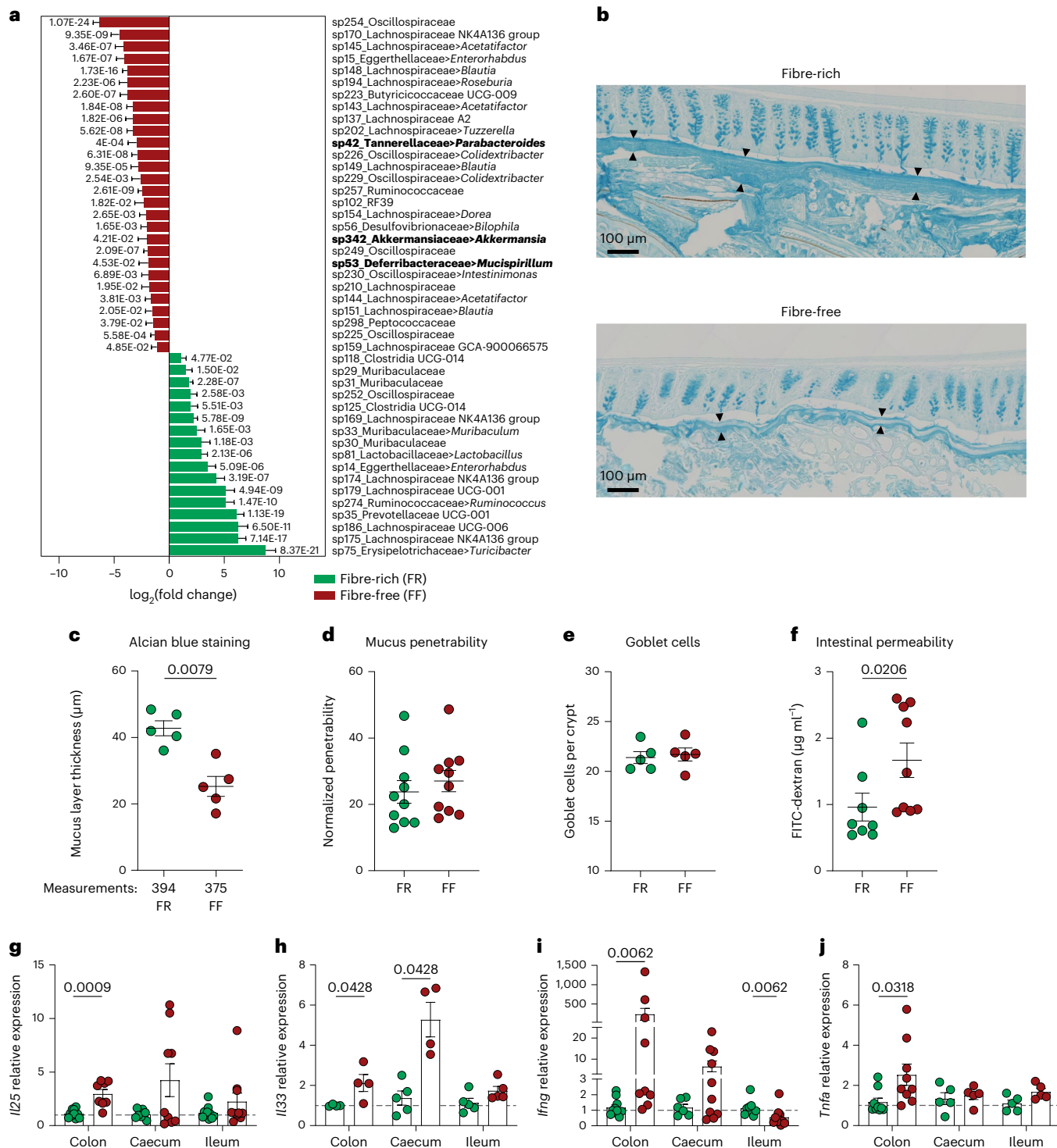


Fig. 1 | Fibre deprivation leads to microbiota-mediated mucosal barrier breakdown. Mice were fed an FR (green dots) or an FF (red dots) diet for 40 days. **a**, Differential abundance analysis of taxa in the faeces of FR-fed mice (green bar) versus FF-fed mice (red bar) ($n = 10$ mice per group, 5 mice per cage, Wald test, P values adjusted using the Benjamini–Hochberg method, features with less than 1 count on average across all samples were excluded). Data are presented as mean \pm s.e.m. Taxa in bold depict known/potential mucin-degrading bacteria; for *Akkermansia*, \sim 1.7-fold increase in FF- compared with FR-fed mice (change from average relative abundance of 1.7% to 5.7%). **b**, Representative images of Alcian blue-stained longitudinal colonic sections of mice fed an FR or FF diet for 40 days. Black arrowheads indicate the edges of the mucus layer ($n = 5$ mice per group). **c**, Mucus layer thickness measured on colonic section stained with Alcian blue. Each dot is the average of several measurements from one animal ($n = 5$ mice per group).

group, two-tailed Mann–Whitney test). The average number of measurements per mouse is indicated on the X axis. **d**, Colonic mucus layer penetrability to 1- μ m-sized beads. Each dot is an average of 4–7 measurements from one animal ($n = 10$ mice per group, two independent experiments). **e**, Goblet cell counts per crypt. Each dot is the average of multiple measurements from one animal ($n = 5$ mice per group). **f**, Intestinal permeability to FITC-dextran ($n = 8$ –9 mice per group, two independent experiments, two-tailed Mann–Whitney test). **g–j**, Relative transcript levels of *I25* (**g**), *I33* (**h**), *Ifng* (**i**) and *Tnfa* (**j**) mRNA in the colon, caecum and ileum. Expression levels were normalized to the FR group, independently for each tissue ($n = 5$ –10 mice per group, two independent experiments, multiple Mann–Whitney, P values adjusted using the Benjamini–Hochberg method). Each dot represents one mouse. All dot plots are represented with mean \pm s.e.m.

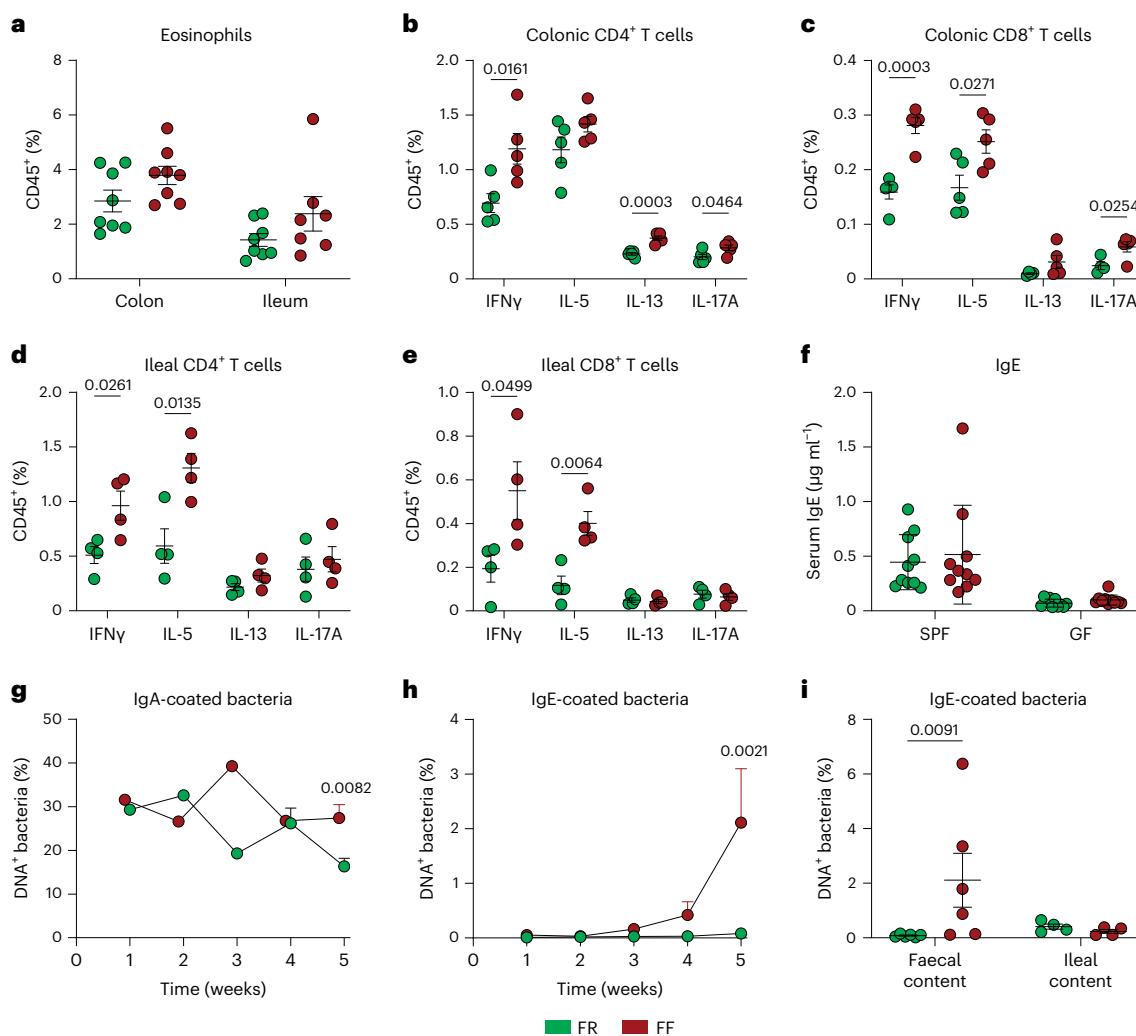


Fig. 2 | Fibre deprivation induces type-2 immune changes in the intestinal mucosa. Mice were fed an FR (green dots) or an FF (red dots) diet for 40 d. **a**, Eosinophil cell frequencies among CD45⁺ single cells in the colonic and ileal lamina propria ($n = 7$ –8 mice per group, two independent experiments, two-way ANOVA, organ effect $P = 0.0018$, diet effect $P = 0.0281$). **b**–**e**, Frequencies of cytokine-expressing colonic CD4⁺ (**b**) and CD8⁺ (**c**) T cells and ileal CD4⁺ (**d**) and CD8⁺ (**e**) T cells among CD45⁺ cells ($n = 4$ –5 mice per group, multiple unpaired *t*-test). **f**, Serum titres of IgE ($n = 9$ –10 mice per group, two independent

experiments, two-way ANOVA). **g**, **h**, Frequencies of faecal IgA-coated (**g**) and IgE-coated (**h**) bacteria over 5 weeks of feeding on FR or FF diet ($n = 1$ –5 mice per group, two-way ANOVA, P values adjusted using the Benjamini–Hochberg method). **i**, Frequencies of faecal and ileal IgE-coated bacteria after 40 d of feeding ($n = 4$ –6 per group, multiple Mann–Whitney test, P values adjusted using the Benjamini–Hochberg method). All dot plots are represented with mean \pm s.e.m.

(Fig. 2f), unsensitized mice treated with PBS showed higher titres when fed FF diet compared with FR diet (Fig. 3f), suggesting that a feeding period longer than 40 d may result in an atopic phenotype. Finally, although serum MCPT1 titres were increased in OVA-CTX sensitized mice compared with OVA- or CTX-treated mice, they remained lower in FF-fed sensitized mice compared with FR-fed sensitized mice, suggesting that cellular pathways alternative to mast cells are involved in worsening food allergy caused by fibre deprivation (Fig. 3g).

We next employed an additional allergen, peanut (PN) (Extended Data Fig. 4a). Neither the diet nor the sensitization affected the weight gain of the mice in the course of the experiment timeline (Extended Data Fig. 4b). FF-fed PN-sensitized (PN-CTX) mice showed more severe symptom scores and temperature drops compared with FR-fed sensitized (PN-CTX) mice (Fig. 3h,i). Although PN-specific IgE and IgG1 were similar between the two diet groups (Extended Data Fig. 4c,d), fibre deprivation increased total IgE and IgG1 levels induced by both PN-CTX or PN sensitization (Extended Data Fig. 4e,f). In addition,

among PN-sensitized mice, FF-fed mice had decreased serum MCPT1 compared with FR-fed mice (Extended Data Fig. 4g), which was similar to the findings from OVA sensitization. As the results between the two food allergens (OVA and PN) were largely consistent, we elected to focus our attention on OVA sensitization for further immune characterizations using CyTOF (Fig. 4a) and Extended Data Fig. 5).

Although the majority of immune cells in the cLP were B cells and regulatory T (Treg) cells (~60% and 5% of CD45⁺ cells, respectively), dietary fibre deprivation mostly affected the proportion of less frequent but inflammatory cells (Fig. 4a). Among OVA-CTX-sensitized mice, the FF diet increased the frequencies of type-2 cells (Th2, ILC2 and mast cells), as well as type-1 (Th1, NK, ILC1 and CD8⁺ T cells) and type-3 cells (Th17, ILC3) (Fig. 4b–j). Although the sensitization tended to decrease the frequencies of Th1 and Th17 cells in FR-fed and FF-fed mice, respectively, the effect of fibre deprivation was also seen in PBS control mice, suggesting a sensitization-independent effect of the diet on the immune landscape (Fig. 4b–j). In addition to inflammatory cells, Treg cells, particularly Gata3⁺ but not Tbet⁺, were more present in the cLP of

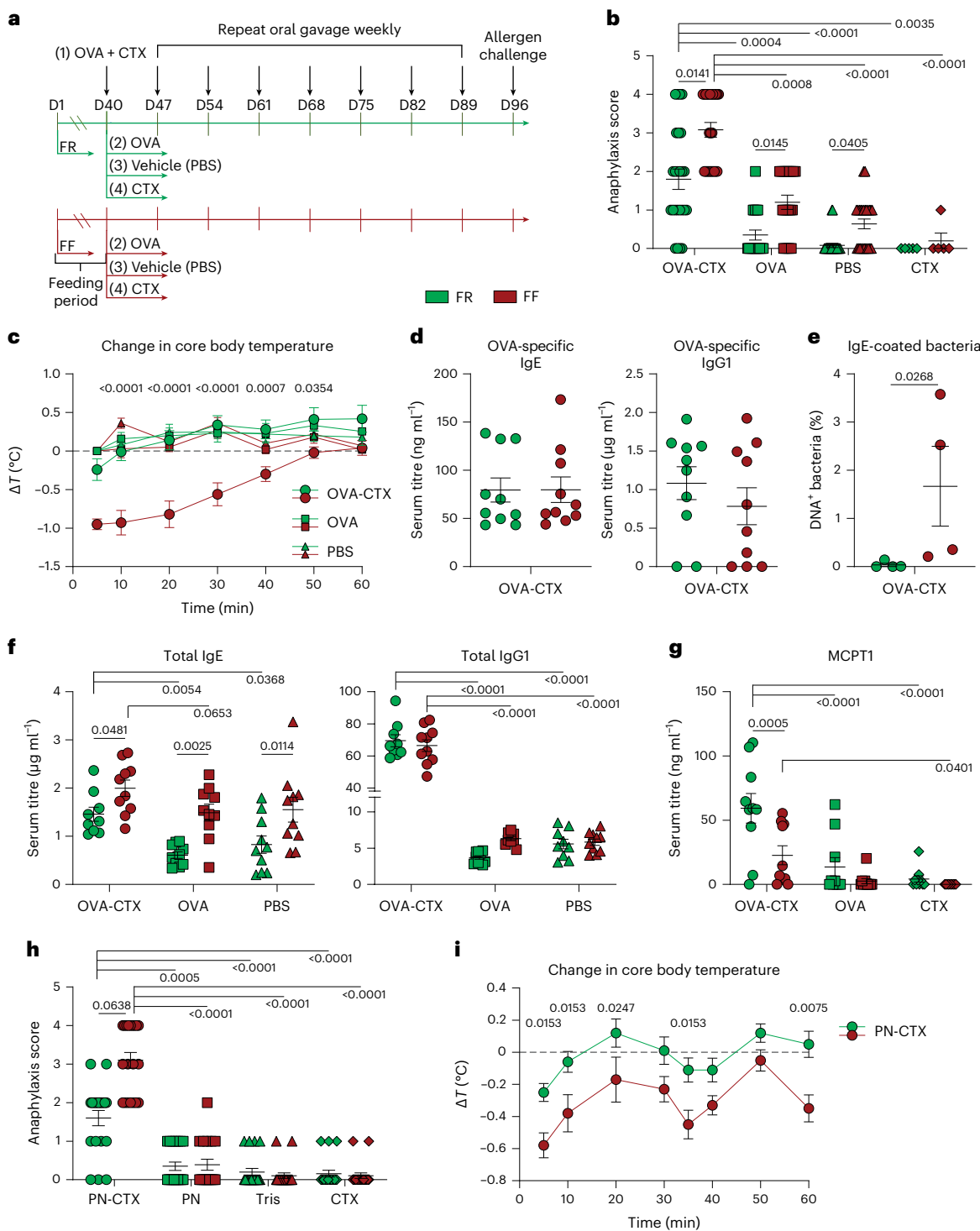


Fig. 3 | Fibre deprivation worsens food allergic responses. **a**, Schematic timeline of OVA sensitization with cholera toxin (CTX) as an adjuvant and control groups. **b,c**, Blinded symptom scores (**b**) and core body temperature (**c**) acquired at OVA challenge ($n = 20$ mice per group, two independent experiments, Kruskal–Wallis test (**b**) or two-way ANOVA (**c**), P values adjusted using the Benjamini–Hochberg method, between FR and FF among OVA-CTX mice). **d**, Serum titres of OVA-specific IgE and IgG1 ($n = 10$ mice per group, two-tailed unpaired t -tests). Note that the titres of both OVA-specific IgE and IgG1 for all other groups were below the limit of detection. **e**, Frequencies of IgE-coated bacteria in the colonic

content of mice at the end of the experiment ($n = 4$ mice per group, two-sided Mann–Whitney test). **f,g**, Serum titres of total IgE and IgG1 (**f**) and mouse mast cell protease 1 (**g**, MCPT1) ($n = 10$ mice per group, two independent experiments, two-way ANOVA, P values adjusted using the Benjamini–Hochberg method). **h,i**, Blinded symptom scores (**h**) and core body temperature (**i**) acquired at peanut (PN) challenge ($n = 20$ mice per group, two independent experiments, Kruskal–Wallis test (**h**) or two-way ANOVA (**i**), P values adjusted using the Benjamini–Hochberg method, between FR and FF among PN-CTX mice). All dot plots are represented with mean \pm s.e.m.

FF-fed mice (Fig. 4f,g). Although typically described as type-1 inflammatory cells, CD8 $^{+}$ T cells have recently been highlighted for their role in food allergy²⁴. Supporting a role in the fibre deprivation-increased

sensitization shown here, IL-5-producing CD8 $^{+}$ T cells, but not CD4 $^{+}$ T cells, were enriched in the cLP of FF-fed OVA-CTX-sensitized mice (Fig. 4k,l).

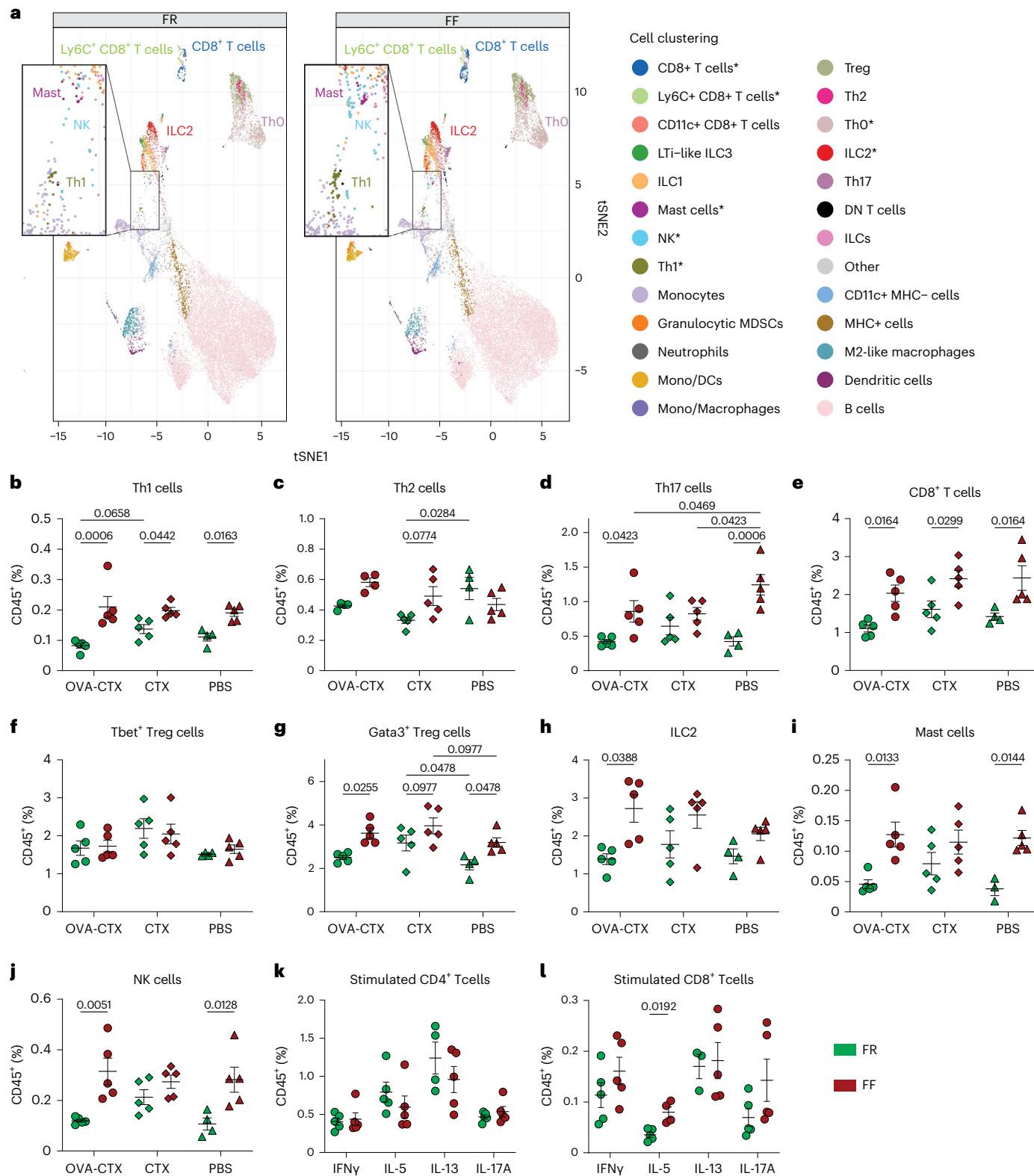


Fig. 4 | Fibre deprivation increases colonic inflammation induced by food allergen sensitization. **a**, UMAP of the main populations identified using FlowSOM among CD45⁺ cells from the colonic lamina propria of FR- and FF-fed OVA-CTX-sensitized SPF mice 24 h after challenge ($n = 5$ per group, multiple Mann–Whitney test, * $P < 0.05$). **b–j**, Frequencies of indicated cell populations among CD45⁺ cells from the colonic lamina propria of FR-fed (green) and

FF-fed (red) mice ($n = 5$ mice per group, two-way ANOVA, unadjusted P values).

k,l, Frequencies of cytokine-expressing CD4⁺ (**k**) and CD8⁺ (**l**) T cells among colonic CD45⁺ cells ($n = 4$ –5 mice per group, multiple unpaired t -test, P values adjusted using the Benjamini–Hochberg method). All dot plots are represented with mean \pm s.e.m.

Allergic sensitization shifts the microbiome in a diet-dependent manner

A microbiome signature has been previously linked with paediatric food allergy²⁵, characterized by increased abundance of the mucin degrader *Ruminococcus gnavus*²⁶ and decreased abundance of several fibre-degrading and probiotic (that is, *Bifidobacterium longum*) species compared with healthy controls²⁵. Nevertheless, it remains unclear whether these microbial changes occur before or as a consequence of allergic sensitization. Faecal microbiome profiles, as summarized by the Bray–Curtis dissimilarity index, were significantly shifted in FR-fed mice upon challenge, but not in FF-fed mice (Fig. 5a). Of note, the microbiome of mice differed mostly depending on the diet (Fig. 5a), suggesting that fibre deprivation itself already creates a stronger selective pressure on the microbiome composition than the sensitization process. Among FR-fed mice, barplots of the relative abundances at the family level revealed increases in the Lachnospiraceae and Peptococcaceae families, and decreases in the families Akkermansiaceae, Bacteroidaceae, Clostridia UCG-014, Muribaculaceae, Prevotellaceae, Tannerallaceae and the order Rhodospirales due to allergic sensitization (Fig. 5b,c).

Differential analysis confirmed significant shifts for 24 features in FR-fed sensitized mice and 7 features in FF-fed sensitized mice (Fig. 5c). Of these, 3 features were significantly changed due to sensitization in FF-fed mice, but not in FR-fed mice, these features belonging either to the genus *Eubacterium* (sp158 and sp169) or to the family Lachnospiraceae (sp139) (Fig. 5c). In contrast, among the features that changed only in FR-fed mice following sensitization, *A. muciniphila* showed the largest shift (Fig. 5c). *A. muciniphila* abundance increased after the 40-day feeding period (pre) and decreased after sensitization (post) in both FR- and FF-fed mice (Fig. 5c). However, while this mucin-degrading bacterium was not detected after sensitization in FR-fed mice, the shift was not as evident in FF-fed mice, probably owing to the mucin-foraging niche created and supported by fibre deprivation (Fig. 5c,d). Consistently, the shift in microbial metabolism under fibre deprivation could be observed similarly before and after sensitization through reduced caecal concentrations of short-chain fatty acids (SCFAs) butyrate, propionate and acetate, and increased concentrations of valerate and protein-derived branched-chain fatty acids (BCFAs) isovalerate and isobutyrate (Fig. 5e). In addition, while BCFA titres increased over the sensitization period in both FR- and FF-fed mice, acetate slightly decreased in FR-fed mice only.

In a previous study, *A. muciniphila* was reported to be decreased in the faecal microbiota of severe asthmatic patients, and oral supplementation of *A. muciniphila* to the native complex gut microbiota was able to modulate the immunophenotype and protect mice from allergic airway inflammation²⁷. By contrast, the abundance of *A. muciniphila* or its family Verrucomicrobiaceae has been reported to be transiently increased in the faeces of food allergic infants by the age of 13–18 months²⁸. Our results show that *A. muciniphila* is lost in sensitized FR-fed mice (Fig. 5c,d); nevertheless, FF-fed mice, which displayed exacerbated food allergy symptoms, did not show a similar complete loss of this bacterium post sensitization (Fig. 5c,d).

A. muciniphila exacerbates food allergic responses under fibre deprivation

To investigate the causal role of *A. muciniphila* in modulating food allergy, we used GF mice colonized with a fully characterized, 14-member synthetic human gut microbiota (14SM) in which *A. muciniphila* can be either included (14SM) or excluded (13SM)¹⁴. In contrast to data in SPF mice (Fig. 5d), *A. muciniphila* was still present in FR-fed mice after sensitization, reaching on average 5–11% of the 14SM community (Fig. 6a and Extended Data Fig. 6). Nevertheless, its relative abundance was still increased in FF-fed mice compared with FR-fed mice, reaching on average 13–18% of the community (Extended Data Fig. 6). In the absence of *A. muciniphila*, the relative abundances of the three other mucin-degrading bacteria, *Bacteroides thetaiotaomicron*,

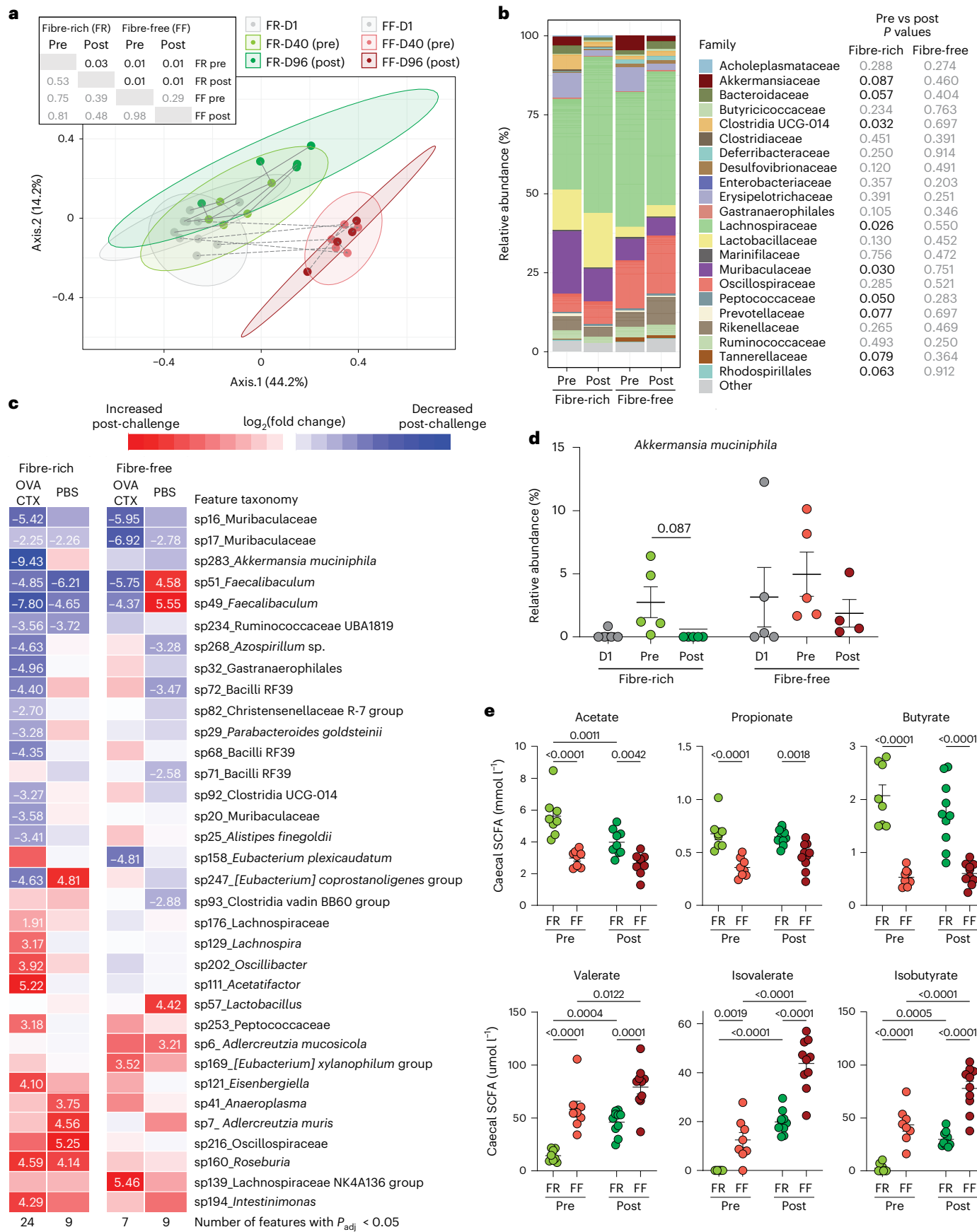
Bacteroides caccae and *Barnesiella intestinihominis*, increased in either both dietary groups or in FF-fed mice (Fig. 6a and Extended Data Fig. 6). The low-abundance bacterium *Marvinbryantia formatexigens* and *Desulfovibrio piger* also substantially expanded in the absence of *A. muciniphila*, in FR-fed and FF-fed mice, respectively (Extended Data Fig. 6), whereas the relative abundance of *Escherichia coli*, *Clostridium symbiosum*, *Bacteroides ovatus*, *Roseburia intestinalis* and *Faecalibacterium prausnitzii* decreased in either both or one of the 13SM dietary groups (Fig. 6a and Extended Data Fig. 6).

As with the SPF mouse data, neither FF feeding nor microbiota composition affected the weight changes in mice during the sensitization period (Extended Data Fig. 7a). In FR diet-fed groups, 14SM-colonized mice treated with OVA-CTX, OVA or CTX did not develop significantly higher symptom scores than PBS control mice, reflective of a moderate model of food allergy symptoms²³ (Fig. 6b). However, FF-fed OVA-CTX and OVA-treated mice had more severe symptoms than CTX- or PBS-treated mice, in addition to FR-fed OVA-CTX and OVA-treated mice (Fig. 6b), reproducing the same pathological profile as seen with SPF mice (Fig. 3b). These results were corroborated by an increased drop in body temperature in FF OVA-CTX mice as compared with FR OVA-CTX mice (Fig. 6c). As previously reported⁷, GF sensitized FR-fed mice exhibited severe anaphylaxis scores at challenge (Fig. 6b). The GF FF-fed mice showed anaphylaxis scores similar to those of the GF FR-fed mice, suggesting that the FF diet alone, without the microbiota, is incapable of further increasing the allergic severity. When comparing FR-fed OVA-CTX-treated mice, both 13SM- and 14SM-colonized mice had reduced disease scores compared with GF mice, supporting the preventive role of the microbiota in the development of food allergy⁷. By contrast, when the mice were fed an FF diet, only 13SM colonization exhibited decreased symptom scores, while 14SM mice had scores as severe as those of GF mice (Fig. 6b).

High levels of MCPT1 were more frequent in OVA-CTX sensitized mice than in OVA-, CTX- or PBS-treated 14SM-colonized mice (Extended Data Fig. 7b). However and unexpectedly, the titres of OVA-specific Ig showed trends opposite to those of the symptom scores among 14SM- and 13SM-colonized mice (Fig. 6b and Extended Data Fig. 7c,d). While the FF-fed 14SM mice were most affected by the allergen challenge, they had lower titres of OVA-specific IgE and IgG1 than the protected 13SM-colonized mice despite higher titres of total IgE and IgG1 (Fig. 6b and Extended Data Fig. 7c–f), indicating that systemic immunoglobulin titres are not good predictors of the severity of allergic responses.

To pinpoint the underlying immune pathways activated by the presence of *A. muciniphila* in the microbiota, we performed CyTOF acquisition of the cLP from these mice (Fig. 6 and Extended Data Figs. 7g–k and 8). Interestingly, while sensitized 14SM-colonized mice were characterized by a strong infiltration of colonic Th2 cells, sensitized 13SM-colonized mice had higher frequencies of Th1, suggesting that *A. muciniphila* within the microbiota promotes the recruitment of Th2 cells during sensitization (Fig. 6d). By contrast, innate type-2 cells (ILC2, M2 macrophages and mast cells) and activated CD69⁺ Th17 cells had the tendency to be more abundant in sensitized 13SM-colonized FR-fed mice than in 14SM-colonized FR-fed mice (Fig. 6e and Extended Data Fig. 7h,i). In 13SM-colonized mice, fibre deprivation decreased the abundances of these innate type-2 cells, as well as CD69⁺ Th17 and Gata3⁺ Foxp3⁺ CD4⁺ T cells, and increased the proportion of Ly6C⁺ CD8⁺ cells (Fig. 6e and Extended Data Fig. 7g–k). In addition, the FF diet increased eosinophil infiltration in 14SM-colonized mice, which was decreased in 13SM-colonized mice (Fig. 6f).

These results support a role for *A. muciniphila* in the maintenance of the allergic type-2 response by promoting Th2 cells under fibre-rich conditions and type-2 innate cells under fibre deprivation, while the 13SM community would have a counteracting effect by supporting the Th1 response. Intriguingly, 14SM-colonized mice exposed to OVA only, without adjuvant, had profiles more similar to OVA-CTX sensitized 13SM-colonized mice than to 14SM-colonized ones, with lower levels of



innate type-2 cells, CD69⁺ Th17 and Gata3⁺ Foxp3⁺ CD4⁺ T cells, and more Ly6C⁺ CD8⁺ T cells under fibre deprivation (Fig. 6e and Extended Data Fig. 7g–k). These data suggest that *A. muciniphila* and CTX cooperate to

modulate these immune cell populations. In another study using FR-fed C57BL/6 mice²⁹, 14SM-colonized mice had more IFNg⁺, IL-17⁺ and RORgt⁺ CD4⁺ T cells than 13SM-colonized mice, suggesting that the Th1/17

Fig. 5 | Food allergen sensitization affects the gut microbiota composition in a diet-dependent manner. **a**, PCoA plot of microbiome profiles using Bray-Curtis dissimilarity index for FR- or FF-fed mice at the beginning of the feeding period (D1), before sensitization (pre, D40) and after sensitization (post, D96). Inset table: *P* values from testing for heterogeneity of dispersion (left of diagonal) and distance between group centroids (right of diagonal). Data for D1 and D40 are shared with a previous study²². **b**, Family-level barplots of relative abundance pooled by diet group and time; *P* < 0.1 indicated with black text colour (*n* = 4–5, multiple paired *t*-tests, all comparisons non-significant after adjustment for multiple comparisons using the Benjamini–Hochberg method). **c**, Heat map of log₂(fold change) of taxonomic features post-challenge (relative to pre-

challenge) among FR- or FF-fed mice that were OVA-sensitized or received PBS as a control. Only those taxa with *P*_{adj} < 0.05 for at least one group are shown. At the bottom of the heat map, the number of features significantly affected by the challenge are listed for each group. **d**, Relative abundance of *A. muciniphila* from the first day of the experiment (D1), from before sensitization (pre) and after sensitization (post) in FR- and FF-fed mice (*n* = 4–5, two-way ANOVA, individual *P* < 0.05, non-significant after *P* values were adjusted using the Benjamini–Hochberg method). **e**, Concentrations of short- and branched-chain fatty acids in the caecal contents of mice before sensitization (pre) and after sensitization (post) (*n* = 8–10, two-way ANOVA, *P* values adjusted using the Benjamini–Hochberg method). All dot plots are represented with mean ± s.e.m.

skewing in the absence of *A. muciniphila* might occur following the sensitization (Extended Data Fig. 9a). Furthermore, in FR-fed C57BL/6 mice colonized without the 10 characterized non-mucin-degrading bacteria, the presence (4SM) or absence (3SM) of *A. muciniphila* did not change the proportion of these populations in the colonic lamina propria, suggesting a role for microbial interactions in the regulation of the mucosal immune profile by *A. muciniphila* (Extended Data Fig. 9a). Finally, as shown in SPF mice, FF diet increased the titres of faecal IgE-coated bacteria in OVA-CTX-sensitized mice (Fig. 6g). In the absence of *A. muciniphila* (13SM), this diet effect was reduced (Fig. 6g).

Since *A. muciniphila* is an abundant mucin-degrading bacterium in the 14SM model, we assessed whether its absence in the 13SM community impaired the overall microbial enzymatic activity of carbohydrate-active enzymes (CAZymes) and sulfatases that are known to be involved in mucin foraging (Extended Data Fig. 9b). As expected, the activity of the plant glycan-targeting β-glucosidase was reduced under fibre deprivation in both 13SM and 14SM FF groups as compared with their FR counterparts. In line with the increased relative abundances of other mucin-degrading bacteria in 13SM groups, differences in the mucin-targeting enzyme activities (β-N-acetylglucosaminidase, α-L-fucosidase and sulfatase) between FR and FF groups within 13SM or 14SM communities remained similar.

Discussion

The canonical pathway of food allergy sensitization begins with allergen sensing by dendritic cells and the release of cytokines that promote the recruitment and activation of type-2 immune cells, which leads to the production of IgE (Extended Data Fig. 10). Later, the IgE-primed mast cells degranulate and induce the allergic reaction as soon as they encounter the allergen. Our results suggest that this model is also largely true in the colonic lamina propria, but tunable by dietary fibre. Fibre deprivation leads to a mixed inflammatory environment comprising innate type-2 cells M2 and ILC2, as well as type-1 cells Th1, NK and CD8⁺ T cells. Although present at low frequencies, these are all key effector cells contributing to increase the pool of cytokines such as IL-5 and IFNy (Fig. 2b,c). The increased secretion of type-2 cytokines, such as IL-5, probably contributes to the eosinophilia and the higher titres of systemic IgE. Interestingly, IFNy was reported to inhibit mouse mast cell degranulation but potentiate FcεRI-mediated antigen endocytosis and presentation^{30,31}, which may explain the lower titres of MCPT1 despite higher frequencies of mast cells in FF-fed mice

before and after sensitization (Fig. 3g and Extended Data Fig. 2c). By contrast, IFNy can induce piecemeal degranulation of eosinophils³². Thus, an immune environment composed of both type-1 and type-2 cells, producing both type-1 and type-2 cytokines, can be seen as an alternative pathway of allergic response in the colon (Extended Data Fig. 10). Intriguingly, allergic gnotobiotic mice recapitulated the symptom profiles of SPF mice, but these were not supported by the systemic titres of OVA-specific IgE. These results beg for an explanation for the role of intestinal IgEs and their antigenic specificity. Although IgE-coated bacteria were recently identified in faecal samples from food allergic children²⁸, the mechanism underlying this process is still elusive. Here we report that fibre deprivation can promote the binding of IgE to gut bacteria, even in the absence of experimental allergic sensitization.

A. muciniphila has been described as having beneficial health effects, in particular by alleviating mucosal permeability³³ and the expression of pro-inflammatory cytokines^{34,35}. Thus, it is currently proposed as a potential probiotic^{36,37}. Our present study shows that the impact of this bacterium is context-dependent and can be detrimental in food allergy when the microbiota is deprived of dietary fibre. In support of our findings, an increase in IL-4 signalling at the transcriptional level in the colon upon monocolonization of GF mice with *A. muciniphila* had previously been reported³⁸, suggesting a role for type-2 immune skewing in the host. Our results also show that *A. muciniphila* colonization supports non-type-2 immune populations CD69⁺ Th17 and Ly6C⁺ CD8⁺ T cells in the colonic lamina propria of FF-fed and FR-fed sensitized mice, respectively (Extended Data Fig. 7j,k). It is likely that there are other commensal gut microbes that can promote tolerance breakdown following dietary changes, either alone or in combination with other species. Identifying such biomarker species and modulating them with dietary intervention would be important in using gut microbiota as a therapeutic/preventative target in food allergy.

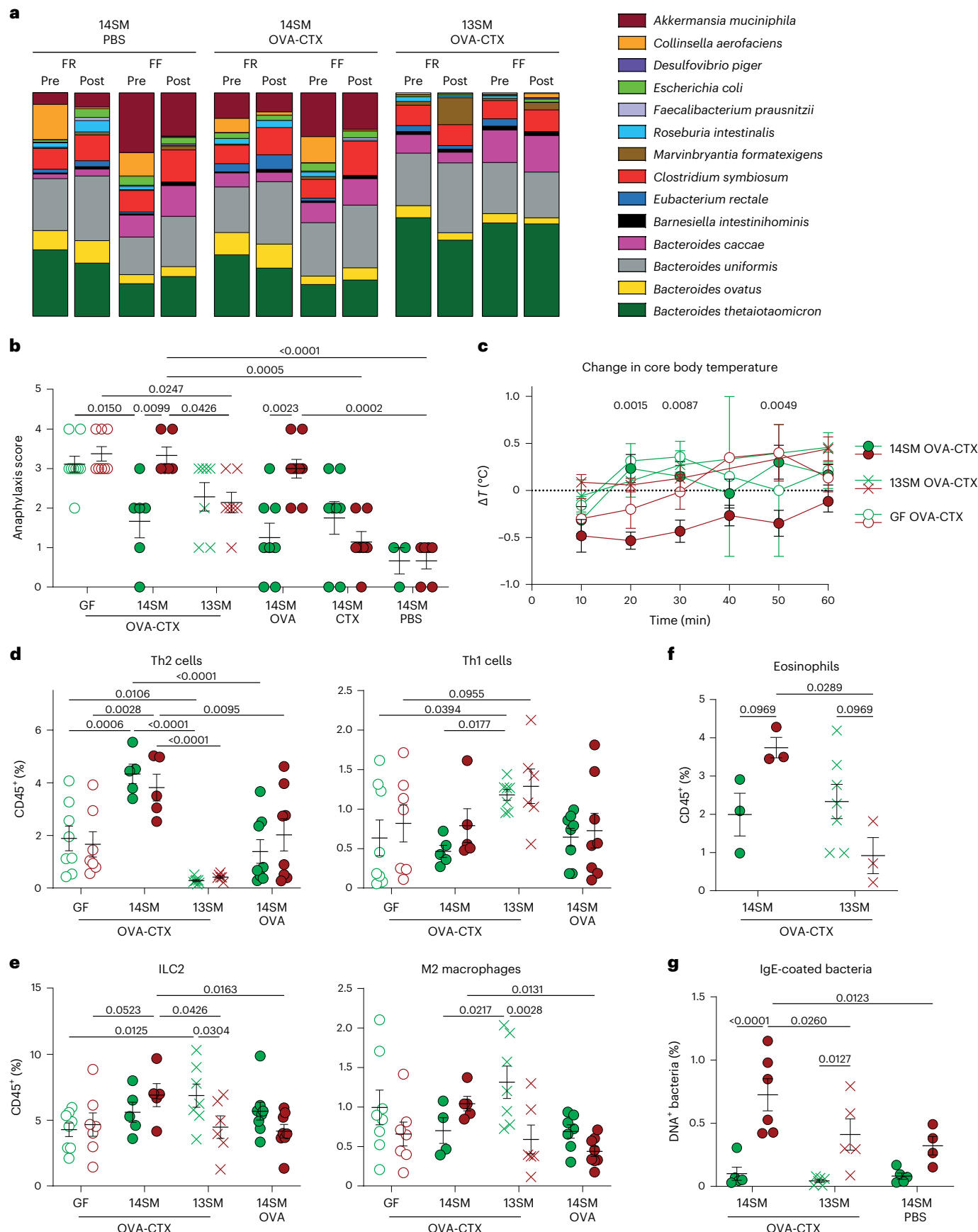
Fibre deprivation increased intestinal permeability in SPF mice, which plays a role in facilitating recognition of food allergens by immune cells. Nevertheless, since the global mucin-degrading capacity of the synthetic community was unchanged in the absence of *A. muciniphila*, these data suggest that increased mucin foraging is not a major driver of the allergic type-2 responses in this model. However, the enhanced mucin-degrading activity of *A. muciniphila* in FF mice may be required as an additional microbial trigger to promote the breakdown of oral tolerance, probably through increased innate type-2

Fig. 6 | *A. muciniphila* exacerbates type-2 immune responses during food allergy under fibre deprivation in a gnotobiotic mouse model. **a**, Relative abundance of microbial strains assessed from pre- and post-sensitization by phylotype-specific qPCR for both 14SM-colonized (left and middle) and 13SM-colonized (right) mice. **b,c**, Blinded symptom scores (**b**) and core body temperature (**c**) acquired after OVA challenge in mice fed an FR (green) or an FF (red) diet (*n* = 3–9, at least two independent experiments, Kruskal–Wallis test with unadjusted *P* values, non-significant after adjustment using the Benjamini–Hochberg method (**b**) or two-way ANOVA (**c**), with *P* values adjusted using the Benjamini–Hochberg method between FR vs FF among OVA-CTX mice).

d–f, Frequencies of immune cell populations identified with mass cytometry and FlowSOM analysis (**d,e**, *n* = 5–10, two independent experiments, two-way ANOVA, non-adjusted individual *P* values, bolded *P* values remain below 0.05 after adjustment using the Benjamini–Hochberg method) and of eosinophils as identified by flow cytometry and FlowJo analysis (**f**, *n* = 3–7, two-way ANOVA, *P* values adjusted using the Benjamini–Hochberg method) in the colonic lamina propria of mice fed an FR or an FF diet. **g**, Frequencies of faecal IgE-coated bacteria at the end of the experiment (*n* = 4–8, two independent experiments, two-way ANOVA, *P* values adjusted using the Benjamini–Hochberg method). All dot plots are represented with mean ± s.e.m.

responses. Although the Th2 response may be dampened by other unknown changes in the 13SM community, such an effect is nonetheless an indirect consequence of the absence of *A. muciniphila*.

Dietary antigens were long thought to be absorbed in the small intestine, where they promote oral tolerance³⁹. In the past decades, however, antigen uptake has been described in the colon through



goblet cell-associated antigen passages⁴⁰, suggesting that allergen sensitization may also develop in the colon. Consistently, our data suggest that the colon is a strategic site for diet–microbiota–mucus interactions and food allergic responses. We have previously identified inflammatory effects of the fibre-deprived diet on the colon²². Here we present evidence that this inflammatory profile may come as a result of barrier breakdown, allowing greater access of luminal antigens to immune cells. Another study identified a link between acute intestinal infection, which caused a barrier break in the colon, and the subsequent onset of a local dietary antigen (OVA) IgE response⁴¹. These data suggest that either an infection- or diet-mediated breakdown in the colonic barrier can drive an immunological response in the form of food allergy. This further supports findings among patients suffering from inflammatory bowel diseases and irritable bowel syndrome, who exhibit a high prevalence of food sensitivity^{42–44}.

An interesting observation in our broad immunophenotyping data in SPF sensitized mice was the immune skewing for both Th2 and Th1/Th17 that is induced by a fibre-deprived diet. In line with this, in atopic dermatitis, acute inflammation transitioning into a chronic stage is characterized by an overall activation of all Th subsets, rather than Th2 to Th1^{45,46}. Allergic inflammation in the fibre-deprived colon can support this phenotype. Overall, our study supports the emerging evidence that food allergy encompasses a vast array of endotypes evolving due to new environmental triggers^{3,4,41,47}. Future clinical evaluation and research should focus on immune distinctions and the site of inflammation between food allergic endotypes to design personalized diet- and microbiota-based therapies.

Methods

Specific-pathogen-free (SPF) experiments

All SPF animal experiment protocols were approved by the Animal Welfare Service at the Luxembourg Institute of Health and further approved by the Veterinary Services Administration within the Ministry of Agriculture (National Authorization No. LUPA2018/18, LUPA2019/29). Sample sizes were pre-determined with the statistician of the Animal Welfare Service. Six-week-old female BALB/c mice were purchased from Charles River Laboratories. Mice were housed in groups of five and assigned randomly to a diet/treatment group. The FR mice were fed the standard CRM (P) rat and mouse breeder and grower diet (Special Diets Services, 801722). The FF diet was custom-manufactured by SAFE diets according to the TD.140343 diet formulation (Envigo), as previously described¹⁴. Mice were provided with their respective diets and autoclaved water ad libitum. For readouts before sensitization, mice were fed for 40 d and then euthanized for tissue/sample processing.

GF and gnotobiotic experiments

All GF and gnotobiotic animal experiment protocols were approved by the Animal Experimentation Ethics Committee at the University of Luxembourg (National Authorization No. LUPA2019/50). The GF status of the mice was verified by culture-based (aerobic and anaerobic) methods. For all gnotobiotic experiments, 6–8-week-old BALB/c mice were housed in isocages in a dedicated axenic room inside a specific opportunistic pathogen-free facility at the University of Luxembourg and were fed the standard diet SAFE R04, irradiated at 40 kGy (SAFE). Mice were colonized with two consecutive daily intragastric gavages of the synthetic microbiota as previously described⁴⁸. One week after the gavage, faecal samples were collected, DNA was extracted and purified, and the colonization of individual strains in the synthetic microbiota was confirmed using phylotype-specific qPCR primers⁴⁸. Diet was switched for half of the cages to the FF diet (irradiated at 25 kGy, SAFE diets) 10 d after colonization.

Allergen sensitization and challenge

The ovalbumin sensitization protocol was adapted from ref. 23 and was conducted as shown in Fig. 3a. All animals started with a feeding period

(40 d for SPF and 7 d for gnotobiotic and GF mice) on either the FR or the FF diet before sensitization. Mice were sensitized by intragastric gavage of 100 µl of the solution related to their treatment group using a reusable 25G feeding needle (FST) once per week for 8 weeks. All solutions were prepared in autoclaved Dulbecco's phosphate-buffered saline (PBS, LOBE17-515F). Treatment groups were as follows: OVA + CTX (100 µg ovalbumin (A5503, Merck), 10 µg cholera toxin (C8052, Merck)), OVA (100 µg ovalbumin), CTX (10 µg cholera toxin) and PBS (PBS alone). One week after the 8th gavage, the mice were challenged with 5 mg of OVA in 200 µl of PBS. During the 1-h challenge period, two researchers performed blinded core body temperature readouts using a rectal probe (BiosebLab) and recorded the clinical symptom score²³. Briefly, '0' was assigned if no symptoms were evident; '1' represents mild scratching, rubbing, or both of the nose, head or feet; '2' and '3' represent intermediate symptoms (for example, oedema around the eyes or mouth, piloerection and/or laboured breathing); '4' represents significantly reduced motility, tremors and/or significant respiratory distress; and '5' represents death. Mice were killed 24 h after the allergen challenge, and samples were collected for analysis.

The peanut sensitization protocol was adapted from ref. 7 and was conducted as shown in Extended Data Fig. 3a. As with the OVA sensitization protocol, all SPF mice started with a 40-day feeding period on either the FR or the FF diet. All solutions were made up in filter-sterilized Tris (20 mM, pH 7.2). Peanut protein was extracted from defatted peanut flour (Bell Plantation)⁷. Mice were sensitized by intragastric gavage of 400 µl of the solution related to their treatment group: PN + CTX (6 mg PN and 10 µg cholera toxin on days 40 and 42, then 6 mg PN and 15 µg cholera toxin), PN (6 mg PN), CTX (10 µg cholera toxin on days 40 and 42, then 15 µg cholera toxin). On day 75, the mice were challenged twice by gavage with 20 mg of PN, 30 min apart. During the 1-h challenge period, two researchers performed blinded core body temperature readouts using a rectal probe and recorded clinical symptom score²³. Mice were killed 3 h after challenge and samples were retrieved for analysis.

Sample processing

All animals were euthanized by cervical dislocation. Blood was extracted immediately by cardiac puncture. Serum was separated by incubating blood samples at 37 °C for 30 min, followed by centrifugation at 845 × g for 30 min. Serum was stored at -20 °C for short-term, or -80 °C for long-term storage.

Colons were removed and placed in either methacarn fixative for mucus layer measurements, or collected in HBSS (w/o) (HBSS without Ca²⁺ and Mg²⁺; LOBE10-543F, Westburg) supplemented with 10 mM HEPES (LOBE17-737E, Westburg) for lamina propria cell isolation. Ileal tissues were collected in HBSS (w/o) for lamina propria cell isolation. Both ilea and colons were processed using the lamina propria dissociation kit (130-097-410, Miltenyi Biotec) and gentleMACS dissociator (Miltenyi Biotec) according to the manufacturer instructions.

Caecal, faecal and ileal contents were collected and flash frozen in liquid nitrogen and stored at -80 °C. Caecal, ileal and proximal colonic tissues were cleaned in PBS and stored in 1 ml RNAProtect tissue reagent (76106, QIAGEN) for up to 1 week, followed by long-term storage at -80 °C.

Mucus layer measurements

After incubation in Methacarnoys fixative¹⁴, colons were stored in methanol until processing. For processing, samples underwent paraffin embedding and thin longitudinal sections of pellet-containing tissue were set on glass slides. Slides were stained with Alcian blue or anti-MUC2 and quantification was performed in a blinded fashion as previously described¹⁴.

For MUC2 staining, the slides were deparaffinized in xylene (28973.328, VWR) 3 times for 5 min at room temperature (r.t.). The same 3 consecutive 5 min washes were repeated with pure ethanol

(10437341, Fisher Scientific) to dehydrate the sections and then with fresh Milli-Q water to wash the slides. To retrieve the antigens from the tissue sections, Retrievagen A pH 6.0 (550524, BD Biosciences) was heated and immediately poured onto the slides and covered to retain the heat as much as possible. After a 10 min incubation, the slides were left to cool in the solution for 20 min. Then the slides were washed in fresh Milli-Q water 3 times for 5 min, incubated in blocking buffer (Tris-buffered saline (TBS) and 10% goat serum (Gibco, 11540526, Fisher Scientific)) for 1 h at r.t., and gently blotted dry. For staining with the primary antibody, the tissue sections on the slides were covered with the rabbit monoclonal anti-MUC2 antibody (ab272692, Abcam, 1/200) in blocking buffer in the dark for 2 h at r.t. The excess liquid was blotted away and the slides were washed by dipping them into fresh TBS for 5 min for 3 consecutive times. The tissue sections were covered with the secondary antibody Alexa Fluor-488-conjugated goat anti-rabbit IgG (H + L) (10 µg ml⁻¹; 10729174, Fisher Scientific) in blocking buffer in the dark for 1 h at r.t. The excess liquid was blotted away and the slides were washed by dipping them into TBS for 3 consecutive times for 5 min. The samples were finally mounted by applying 2–3 drops of ProLong gold antifade mountant with DAPI (Invitrogen, 11549306, Fisher Scientific) and a cover slip to the colon section. After incubating for 24 h at r.t., the slides were sealed using nail varnish and stored in the dark at 4 °C until they were visualized on the Axio Observer Z1 inverted fluorescence microscope (Carl Zeiss). Images were analysed using the MATLAB software BacSpace¹⁵ to determine mucus layer thickness exclusively in pellet-containing sections. MUC2⁺ goblet cells per crypt were counted by two independent persons using the ImageJ software (<https://imagej.nih.gov/>).

Mucus penetrability assay

Penetrability of the colonic mucus was assessed as previously described²⁰. Briefly, colons were flushed with ice-cold oxygenated KREBS buffer ‘Transport’ (116 mM NaCl, 1.3 mM CaCl₂, 3.6 mM KCl, 1.4 mM KH₂PO₄, 23 mM NaHCO₃ and 1.2 mM MgSO₄; Carl Roth) and opened along the mesenteric axis. The longitudinal muscle layer was removed by blunt dissection and the distal mucosa was inserted in a perfusion chamber. The basolateral chamber was filled with 0.6 µg ml⁻¹ SYTO9 (Fisher Scientific, 10237582) in oxygenated KREBS ‘Base’ glucose buffer (KREBS ‘Base’ buffer: 136 mM NaCl, 1.5 mM CaCl₂, 4.3 mM KCl, 1.6 mM KH₂PO₄, 27.1 mM NaHCO₃ and 1.4 mM MgSO₄; KREBS glucose buffer: 10 mM glucose, 5.7 mM sodium pyruvate and 5.1 mM sodium-L-glutamate in KREBS ‘Base’ oxygenated buffer; Carl Roth), and the apical chamber was filled with oxygenated KREBS mannitol buffer (containing 10 mM mannitol, 5.7 mM sodium pyruvate and 5.1 mM sodium-L-glutamate in KREBS ‘Base’ oxygenated buffer). After 10 min incubation in the dark at r.t., excess KREBS mannitol buffer was removed and FluoSphere carboxylate beads (1 µm, red 580/605, Invitrogen, F882) were applied on top and allowed to sediment on the tissue for 5 min in the dark at r.t. The apical chamber was then gently washed several times with KREBS mannitol buffer to remove excess beads. The chamber was incubated for 10 min in the dark before being visualized with an Axio Examiner KMAT microscope (Carl Zeiss) using the Zen3.0 (Blue Edition, Carl Zeiss) software. For each tissue, 4–7 confocal images were taken in XY stacks from the epithelium at the bottom to the beads on top, with 5-µm intervals between sections. Images were then analysed with Imaris software (Oxford Instruments Imaris). Penetrability was computed as the area under the curve to the peak of bead frequency as a function of the distance from the epithelium (Extended Data Fig. 1c). The same method was used to compute mucus thickness as the distance between the median position of the beads and the median position of the epithelium (Extended Data Fig. 1c,d).

Intestinal permeability assay

Mice were fasted for 4 h before the assay, followed by oral gavage with FITC-dextran (FD4-250MG, Merck) solution (100 mg ml⁻¹ in PBS) so that

they received 44 mg FITC-dextran per 100 g of body weight. The mice were anaesthetized 4 h later by intraperitoneal injection of ketamine (12.5 mg per 100 g body weight) and medetomidine (0.025 mg per 100 g body weight), and blood was collected via cardiac puncture in a 1.5 ml tube protected from light. Serum was separated by incubating blood samples at 37 °C for 30 min, followed by centrifugation at 845 × g for 30 min. Serum (100 µl) diluted with an equal volume of PBS was added to a 96-well black/clear flat-bottom polystyrene microplate (655906, Greiner). The concentration of FITC in serum was determined by spectrophotofluorometry at an excitation of 485 nm (20 nm band width) and an emission wavelength of 528 nm (20 nm band width), using serially diluted FITC-dextran (0, 125, 250, 500, 1,000, 2,000, 4,000, 6,000, 8,000 ng ml⁻¹) as a standard. Serum from mice not administered with FITC-dextran was used to determine the background.

Bacterial genomic DNA extraction and qPCR analysis

Bacterial DNA was extracted from faecal pellets using phenol-chloroform extraction. Faecal pellets were disrupted in a mix of 500 µl buffer A (200 mM NaCl, 200 mM Tris, 20 mM EDTA), 210 µl 20% SDS, 500 µl equal parts phenol:chloroform and ~250 µl acid-washed glass beads (G1277, Merck) per sample. Mechanically lysis was performed on a Mixer Mill MM 400 (Retsch, Fisher Scientific) for 5 min at 30 Hz, then samples were centrifuged at 18,000 × g for 3 min at 4 °C. The aqueous phase was recovered and 500 µl phenol:chloroform was added, mixed by inversion and then centrifuged at 18,000 × g for 3 min at 4 °C. The aqueous phase was recovered and 500 µl pure chloroform was added. Samples were mixed by inversion and then centrifuged at 18,000 × g for 3 min at 4 °C. The aqueous phase was recovered into a new tube and 1 volume of isopropanol and 1/10 volume 3 M sodium acetate (pH 5.2) were added. Samples were stored at -20 °C for 1 h, followed by centrifugation at maximum speed for 20 min at 4 °C. The supernatants were discarded and the DNA pellets were further cleaned with 1 ml 70% ethanol. Pellets were air-dried for ~1 h and then resuspended in 100 µl of ultrapure water (Invitrogen, 12060346, Fisher Scientific). The DNA was purified using QIAGEN DNeasy blood and tissue kit (69506, QIAGEN) according to manufacturer instructions. Final quantification was performed with a NanoPhotometer N60 (Implen, Fisher Scientific).

DNA (20 ng) was amplified in 12.5 µl of master mix: buffer (10966034, Invitrogen), 1.5 mM MgCl₂ (10966034, Invitrogen), 200 µM dNTP (10297117, Invitrogen), GelStar nucleic acid gel stain (Lonza, LONZ50535, VWR), 0.5 U Platinum Taq DNA polymerase (10966034, Invitrogen) and 0.2 µM each of forward and reverse primers¹⁴. The qPCR cycle consisted of pre-denaturation at 95 °C for 3 min, followed by 40 cycles of 3 s denaturation at 95 °C, 20 s annealing at 55 °C and 20 s extension at 68 °C. Samples were held at 95 °C for 15 s post-extension and then a melting curve was generated by heating from 60 °C to 95 °C, with 0.3 °C interval increases over 15 s.

16S ribosomal RNA gene sequencing and analysis

Bacterial DNA concentrations were measured using a Qubit dsDNA HS assay kit (Q32854, Invitrogen) on a Qubit4 fluorometer (Q33238, Invitrogen). The V4 region of the 16S rRNA gene was amplified using dual-index primers⁴⁹ and sequenced on an Illumina MiSeq system at the Integrated BioBank of Luxembourg (IBBL, Dudelange, Luxembourg). Raw sequences were processed using QIIME 2 (v.2020.6)⁵⁰ with DADA2 for sequence quality control. Sequences were aligned and taxonomic assignment was performed using VSEARCH against the SILVA 138 reference database⁵¹. A range of 13,769–31,494 reads were obtained per sample (median frequency of 20,029), corresponding to 4,602 features or 345 genera. Data were filtered by removing genera with less than 1 count on average, yielding 214 genera in subsequent analyses. Principal coordinates analysis (PCoA) plots were generated in RStudio v.1.3.1093 (R v.4.0.2) using the package ‘vegan’ (v.2.5-7)⁵², with clustering significance testing using the betadisper() function in vegan and the pairwise.

adonis() function in the package ‘pairwiseAdonis’ (v.0.4)⁵³ to test for heterogeneity of dispersion and difference in centroids, respectively. Relative abundance plots were generated using the package ‘phyloseq’ (v.1.34.0)⁵⁴ and ‘ggplot2’ (v.3.3.5)⁵⁵. The package ‘DESeq2’ (v.1.30.1)⁵⁶ was used to perform differential abundance analyses.

RNA extraction

Tissues were thawed on ice in 1 ml of TRIzol reagent (15596026, Life Technologies). A 0.5-mm metal bead (69989, QIAGEN) was added before mechanical lysis on a Mixer Mill MM 400 (Retsch, Fisher Scientific) for 8–10 min at 30 Hz. The extraction was performed according to the TRIzol reagent protocol with a few adaptations. After bead beating, samples were centrifuged at 12,000 × g for 5 min at 4 °C. The supernatant was transferred into a fresh tube and 200 µl of pure chloroform was added. Samples were mixed by shaking for 15 s and left to incubate for 3 min at r.t., then centrifuged at 12,000 × g for 15 min at 4 °C. The aqueous phase was added to 500 µl isopropanol in a new tube, mixed by shaking for 10 s and left to incubate for 10 min at r.t. The samples were then centrifuged for 10 min at 12,000 × g at 4 °C for the precipitation of total RNA. Supernatant was removed and samples were washed with 1 ml cold 75% ethanol. The pellets were left to dry at 37 °C for 5–10 min. Pellets were resuspended in 50 µl nuclease-free water and incubated at 56 °C for 15 min. A DNase treatment was performed following the Thermo Scientific DNase I, RNase-free (EN0521, Thermo Scientific,) protocol, followed by purification with QIAGEN RNeasy mini kit (74106, QIAGEN) according to manufacturer instructions. Final RNA concentrations were quantified using a NanoPhotometer N60 (Implen). Reverse transcription was performed according to the Invitrogen Superscript IV reverse transcriptase protocol (18090010, Invitrogen) in combination with RNaseOUT (10777019, Invitrogen).

Cytokine gene expression

qPCR reactions were performed using SYBR Green detection method and Platinum *Taq* DNA polymerase kit (Invitrogen) on a C1000 Touch thermal cycler (Biorad). Before qPCR, complementary DNA samples were diluted 1/5 in 80 µl of nuclease-free water. cDNA (1 µl) was amplified with 11.5 µl of master mix containing buffer (10966034, Invitrogen), 2.5 mM MgCl₂ (10966034, Invitrogen,), 400 µM dNTP (1029711, Invitrogen), GelStar nucleic acid gel stain (Lonza, LONZ50535, VWR), 0.5 U Platinum *Taq* DNA polymerase (10966034, Invitrogen) and 0.2 µM each of forward and reverse primers. The qPCR cycle consisted of pre-denaturation at 94 °C for 5 min, followed by 40 cycles of 20 s denaturation at 94 °C, 50 s annealing at 60 °C and 45 s extension at 72 °C. Samples were held at 72 °C for 5 min post-extension and then a melting curve was generated by heating from 65 °C to 95 °C with 0.3 °C interval increases over 15 s. mRNA cytokine expression was normalized to the expression of GAPDH. The following primers (Kaneka Eurogentec) were used: *Ifng* forward (5'-ATGAACGCTACACACTGCATC-3'), *Ifng* reverse (5'-CCATCCTTTGCCAGTCCTC-3'); *Il22* forward (5'-GC AGCGTACATCGTCAACC-3'), *Il22* reverse (5'-TCCCCGATGAGGCC GGACA-3'); *Il25* forward (5'-ACAGGGACTTGAATGGGTC-3'), *Il25* reverse (5'-TGGTAAAGTGGACGGAGTTG-3'); *Il33* forward (5'-AA CTCCAAGATTCCCCGGC-3'), *Il33* reverse (5'-TTATGGTGAGGCCA GAACGG-3'); *Tslp* forward (5'-ACGGATGGGGCTAACTTACAA-3'), *Tslp* reverse (5'-AGTCCTCGATTGCTCGAAC-3'); *Tnfa* forward (5'-AGCCCACGTCGTAGCAAAC-3'), *Tnfa* reverse (5'-GATAGCAAT CGGCTGACGG-3'); *Il5* forward (5'-AGGCTTCCGTCCCTACTCAT-3'), *Il5* reverse (5'-TACCCCCACGGACAGTTGA-3'); *Il17a* forward (5'-TACCTCAACCGTCCACGTC-3'), *Il17a* reverse (5'-TCCCCCTCCG CATTGACACAG-3'); *Il17f* forward (5'-TGAAGTGCACCCGTGAAACA-3'), *Il17f* reverse (5'-GCTACCTCCCTCAGAATGGC-3'); *Muc2* forward (5'-GACGGCGATGTCTACCGATT-3'), *Muc2* reverse (5'-CCAGCTTGT GGGTGAGGTAG-3'); *Gapdh* forward (5'-AATTCAACGGCACAGTCAA GGC-3'), *Gapdh* reverse (5'-GTGGTTCACACCCATCACAAA-3'). Samples showing aberrant melting curves were excluded from the analysis.

CyTOF

To examine the immunological landscape behind the increased allergic phenotype, we performed broad immunophenotyping of the cLP by CyTOF using a 28-marker panel. Single-cell suspension of colonic lamina propria cells were stained with a 28-marker panel as previously described²². Briefly, 3 × 10⁶ cells were stained with 5 µM cisplatin solution (201064, Fluidigm) for 5 min. Cells were washed in FACS buffer (PBS, 2% FBS, 2 mM EDTA) and extracellular cell surface staining mix was added for 30 min at r.t. (Supplementary Table 1). Cells were washed twice, fixed using the Foxp3 Transcription Factor Staining buffer set (eBioscience, 00-5523-00, Life Technologies) for 45 min at 4 °C and washed in the permeabilization buffer. The intracellular cell staining mix was added to the cells for 30 min at r.t. (Supplementary Table 1). Samples were washed twice in FACS buffer, resuspended in Cell-ID Intercalator-Ir (201192A, Fluidigm) in MaxPar fixation solution (201192 A, Fluidigm) and refrigerated overnight, or for up to 5 d. Before data acquisition on the Helios mass cytometer (Fluidigm), samples were washed twice in PBS and then twice in deionized water. Samples were resuspended in deionized water at 0.5 × 10⁶ cells per ml, with 10% calibration beads (EQ Four Element Calibration Beads, 201078, Fluidigm). Normalized FCS files were imported in FlowJo v.10.8.1 (BD Life Sciences). The files were cleaned to exclude calibration beads and doublets, and CD45⁺ cells were exported as new files, which were later imported into RStudio (v.1.0.143, R v.3.4.4) using the R package flowcore (v.1.44.2) and FlowSOM (v.2.6.0) for unsupervised analysis, following a previously described pipeline^{57,58}. We performed FlowSOM⁵⁹ clustering (Extended Data Fig. 5) and generated a uniform manifold approximation and projection (UMAP)⁶⁰ plot to visualize the cell populations contributing to the immune landscape within the cLP (Fig. 4a).

Cell stimulation and flow cytometry

Before staining for cytokines, single-cell suspensions from ileal and colonic lamina propria were incubated for 4 h at 37 °C in 5% CO₂, with lymphocyte activation cocktail (423304, Biolegend) in DMEM (LOBE12-604F, Westburg,) complemented with 10% FBS, 100 U ml⁻¹ penicillin/streptomycin (LOBE17-602E, Westburg), glutamine (LOBE17-605E, Westburg), 10 mM HEPES (LOBE17-737E, Westburg) and 0.1% β-mercaptoethanol (M6250, Merck). For eosinophils and cytokine expression analysis, cells were washed with PBS and incubated with Zombie NIR (423105, Biolegend) for 15 min at 4 °C before fixation with Cytofix/Cytoperm solution kit (BD Biosciences). Cells were then washed with FACS buffer, incubated with Fc block (1 µg per 10⁶ cells, 553142, BD Biosciences) for 15 min and stained with the antibody mix (Supplementary Table 1) for 30 min at 4 °C. Samples were finally washed and resuspended in PBS for acquisition on a NovoCyte Quanteon flow cytometer (ACEA Biosciences). FCS files were analysed in FlowJo v.10.8.1 (BD Biosciences). For each reported population, counts were normalized to the LD⁻CD45⁺/Single Cells/Width, SSC-H subset and results are presented as a percentage of CD45⁺ cells.

Lipocalin-2 ELISA

Faecal samples were resuspended in 500 µl ice-cold PBS with 1% Tween-20, followed by agitation at 2,000 r.p.m. for 20 min at 4 °C on a thermomixer (Eppendorf). Samples were then centrifuged for 10 min at 21,000 × g at 4 °C. Supernatants were stored at -20 °C until further analysis. Lipocalin-2 detection was performed using the mouse Lipocalin-2/NGAL DuoSet ELISA (R&D Systems, DY1857, Bio-Techne) according to manufacturer instructions.

MCPT1 ELISA

Mouse MCPT1 was detected in serum samples using the MCPT1 Mouse Uncoated ELISA kit (88-7503-88, Life Technologies) according to manufacturer instructions, but adapted for 384-well microplates.

Allergen-specific ELISA

Allergen-specific IgE and IgG1 antibodies were quantified from serum samples by sandwich ELISA. For OVA-specific assays, 20 µl of ovalbumin (A5503, Merck) at 100 ng µl⁻¹ in PBS were added to each well of a 384-well microplate (781061, Greiner Bio-One) and incubated overnight at 4 °C. Wells were washed 4 times with 100 µl of wash buffer (1% Tween-20, 154 mM sodium chloride and 10 mM Tris-ma-base) and blocked with 75 µl of blocking buffer (15 mM Trizma-acetate, 136 mM sodium chloride, 2 mM potassium chloride and 1% (w/v) BSA (bovine serum albumin)) for 2 h at r.t. Undiluted mouse sera were used to determine the OVA-specific IgE antibody concentrations, using the mouse anti-ovalbumin IgE monoclonal antibody (Clone E-C1, 7091, Ams Biotechnology) as serially diluted standard (range 0–1,000 pg µl⁻¹) in dilution buffer (DB; 15 mM Trizma-acetate, 136 mM sodium chloride, 2 mM potassium chloride, 0.1% (w/v) Tween-20 and 1% BSA). To determine the OVA-specific IgG1 antibody concentrations, mouse sera were serially diluted from 1/400 to 1/12,800 in DB. The mouse anti-ovalbumin IgG1 monoclonal antibody (Clone L71, 7093, Ams Biotechnology) was used as serially diluted standard (range 0–1,000 pg µl⁻¹) in DB. After a washing step performed as described above, 20 µl of diluted standards and samples were added to corresponding wells. The plate was then incubated for 90 min at r.t. The washing step was repeated and 20 µl of detection antibody, either the phosphatase alkaline-conjugated goat anti-mouse IgE (SouthernBiotech, 1110-04, ImTec Diagnostics) or the phosphatase alkaline-conjugated goat anti-mouse IgG1 (SouthernBiotech, 1071-04, ImTec Diagnostics) diluted 1/500 in DB, were added to each corresponding well. The plates were then incubated for 90 min at r.t. Following a last wash, 40 µl of substrate (1x phosphate tablet, S0942, Merck) dissolved in 10 ml of substrate buffer (1 mM 2-amino-2-methyle-1-propanol, 0.1 mM MgCl₂ × 6H₂O) were added to each well. After a last incubation step for 60 min at 37 °C, the absorbance was measured at 405 nm using an ELISA plate reader (SpectraMax Plus 384 microplate reader and SoftMax Pro 7 software, Molecular Devices). The OVA-specific IgE or IgG1 antibody concentrations were determined for each sample using the corresponding formulated standard curve.

For PN-specific assays, the same protocol was used with adapted antigen. Peanut protein extracted from defatted peanut flour¹⁰ (Bell Plantation) and diluted at 12.5 ng µl⁻¹ in carbonate-bicarbonate buffer (C3041, Merck) was used for the coating overnight. Mouse sera were diluted 1/10 in DB to determine PN-specific IgE antibody levels and 1/100 to determine PN-specific IgG1 antibody levels. Both detection antibodies (goat anti-mouse IgE-phosphatase alkaline-conjugated and goat anti-mouse IgG1-phosphatase alkaline-conjugated (SouthernBiotech, ImTec Diagnostics)) were diluted 1/1,000 in DB. Absorbance was measured at 405 nm using an ELISA plate reader (SpectraMax Plus 384 microplate reader and SoftMax Pro 7 software, Molecular Devices).

Total IgE and IgG1 ELISA

Total IgE and IgG1 were quantified from serum samples by sandwich ELISA. The same protocol as for allergen ELISA was used, with adapted reagents. Rat anti-mouse IgE at 60 ng per well or rat anti-mouse IgG1 at 20 ng per well (SouthernBiotech, 1130-01 and 1144-01 respectively, ImTec Diagnostics) was diluted in carbonate buffer and used as capture antibody. Mouse sera were serially diluted from 1/10 to 1/320 to determine the total IgE antibody concentrations, and the mouse IgE isotype control (SouthernBiotech, 0114-01, ImTec Diagnostics) was used as the serially diluted standard in DB (range 0–250 pg µl⁻¹). To determine the total IgG1 antibody concentrations, mouse sera were serially diluted from 1/500 to 1/16,000 in DB, and the mouse IgG1 isotype control (SouthernBiotech, 0102-01, ImTec Diagnostics) was used as the serially diluted standard in DB (range 0–2,000 pg µl⁻¹). Each detection antibody, either the phosphatase alkaline-conjugated goat anti-mouse IgE (SouthernBiotech, 1110-04, ImTec Diagnostics) or the phosphatase alkaline-conjugated goat anti-mouse IgG1 (SouthernBiotech, 1071-04, ImTec Diagnostics), was diluted 1/500 in DB for the assays. The total IgE

or IgG1 concentration was calculated the same way as the OVA-specific IgE/IgG1 concentration.

SCFA quantification

Metabolomics analysis was performed on flash-frozen caecal content. For each sample, approximately 50 mg of caecal contents was mixed with 500 µl Milli-Q water with 2-ethylbutyric acid. Samples were homogenized using 1.4 mm ceramic beads, centrifuged at 21,000 × g for 5 min at 4 °C and run on GC–MS according to ref. 61.

Flow cytometry for Ig-coated bacteria

Quantification of Ig-coated bacteria was performed from frozen faecal samples or tissue contents by flow cytometry. Samples were homogenized in 500 µl ice-cold PBS by mixing at maximum speed on a ThermoMixer for 20 min at 4 °C. Samples were topped up with 500 µl PBS, followed by centrifugation at 100 × g for 5 min at 4 °C. The supernatant was passed through a 70-µm strainer (Pluriselect, 43-10070-70, ImTec diagnostics), followed by centrifugation at 10,000 × g for 5 min at 4 °C. The pellet was resuspended with 1 ml PBS for measurement of the optical density at 600 nm and quantification of the bacteria. Approximately 10⁹ bacteria were used per staining. Samples were incubated with 500 µl PBS with 5% goat serum (Gibco, 11540526, Fisher Scientific) at 4 °C for 20 min. After centrifugation at 10,000 × g for 5 min at 4 °C, pellets were resuspended in PBS with 5% goat serum and the appropriate antibody: FITC-conjugated anti-mouse IgA (Clone mA-6E1, eBioscience, 11-4204-83, Life Technologies), PE-conjugated anti-mouse IgE (Clone RME-1, 406908, Biolegend) or PE-conjugated IgG1 isotype (Clone RTK2071, 400408, Biolegend). After incubating for 30 min at 4 °C, samples were washed in 1 ml PBS. Bacterial pellets were resuspended in 200 µl DNA staining solution (0.9% NaCl in 0.1 M HEPES, pH 7.2) with 1:4,000 SYTO 60 red fluorescent nucleic acid stain (5 mM solution in DMSO, S11342, Invitrogen) and incubated for 20 min at 4 °C. Samples were washed in 1 ml PBS and resuspended in 200 µl PBS for data acquisition on a NovoCyte Quanteon flow cytometer (ACEA Biosciences). FCS files were imported into FlowJo v.10.8.1 (BD Biosciences) for analysis. IgE-coated bacteria were quantified using a negative gate constructed with the corresponding isotype control sample (Extended Data Fig. 2d).

p-nitrophenyl-based enzyme assays

The enzyme assays to quantify the activities of β-glucosidase β-N-acetyl-glucosaminidase, α-L-fucosidase and sulfatase in faecal pellets of 14SM and 13SM OVA-CTX mice fed an FR or FF diet were performed following a previously described protocol⁶². Data were excluded in cases where insufficient quantities of protein were extracted from the faecal supernatant (β-glucosidase: n = 1 among 13SM OVA-CTX FR-fed mice; α-L-fucosidase: n = 3 among 13SM OVA-CTX FF-fed mice; sulfatase: n = 2 among 14SM OVA-CTX FF-fed mice, n = 2 among 13SM OVA-CTX FR-fed mice and n = 2 among 13SM OVA-CTX FF-fed mice). Note that the enzyme activities reported here are not to be considered as absolute enzyme activities but are important for relative comparisons between different groups.

Statistical analysis

Unless otherwise specified, all statistical analyses were performed in GraphPad Prism v.8.0 and 9.0. Normality tests were performed to verify the distribution of data. Outliers were removed using the ROUT test (Q = 2%). Comparisons were performed using either an unpaired t-test, a Mann–Whitney test, a two-way ANOVA or a Kruskal–Wallis test, with P values adjusted using the Benjamini–Hochberg method. For each graph, one dot represents one mouse and the number of mice per group (n) is indicated in the legend.

Reporting summary

Further information on research design is available in the Nature Portfolio Reporting Summary linked to this article.

Data availability

The raw fastq files from 16S rRNA gene sequencing have been deposited in the European Nucleotide Archive (ENA) at EMBL-EBI under accession numbers [PRJEB53451](https://www.ebi.ac.uk/ena/browser/view/PRJEB53451) (<https://www.ebi.ac.uk/ena/browser/view/PRJEB53451>) and [PRJEB51707](https://www.ebi.ac.uk/ena/browser/view/PRJEB51707) (<https://www.ebi.ac.uk/ena/browser/view/PRJEB51707>). We used the SILVA 138 SSU Ref NR 99 database. The mass cytometry datasets for colonic lamina propria have been uploaded to the FlowRepository database under accession number FR-FCM-ZSG2 (<https://flowrepository.org/id/FR-FCM-ZSG2>).

Code availability

The CyTOF analysis pipelines used in this study can be found at <https://github.com/DII-LIH-Luxembourg/amuc-allergy>.

References

- Gupta, R. S. et al. Prevalence and severity of food allergies among US Adults. *JAMA Netw. Open* **2**, e185630 (2019).
- Gupta, R. S. et al. The prevalence, severity, and distribution of childhood food allergy in the United States. *Pediatrics* <https://doi.org/10.1542/peds.2011-0204> (2011).
- Akdis, C. A. Does the epithelial barrier hypothesis explain the increase in allergy, autoimmunity and other chronic conditions? *Nat. Rev. Immunol.* <https://doi.org/10.1038/s41577-021-00538-7> (2021).
- Renz, H. & Skevaki, C. Early life microbial exposures and allergy risks: opportunities for prevention. *Nat. Rev. Immunol.* **21**, 177–191 (2021).
- Plunkett, C. H. & Nagler, C. R. The Influence of the microbiome on allergic sensitization to food. *J. Immunol.* <https://doi.org/10.4049/jimmunol.1601266> (2017).
- Feehley, T. et al. Healthy infants harbor intestinal bacteria that protect against food allergy. *Nat. Med.* **25**, 448–453 (2019).
- Stefka, A. T. et al. Commensal bacteria protect against food allergen sensitization. *Proc. Natl Acad. Sci. USA* **111**, 13145–13150 (2014).
- Hussain, M. et al. High dietary fat intake induces a microbiota signature that promotes food allergy. *J. Allergy Clin. Immunol.* <https://doi.org/10.1016/j.jaci.2019.01.043> (2019).
- Tan, J. et al. Dietary fiber and bacterial SCFA enhance oral tolerance and protect against food allergy through diverse cellular pathways. *Cell Rep.* **15**, 2809–2824 (2016).
- Johansson, M. E. V. & Hansson, G. C. Immunological aspects of intestinal mucus and mucins. *Nat. Rev. Immunol.* **16**, 639–649 (2016).
- Martens, E. C., Neumann, M. & Desai, M. S. Interactions of commensal and pathogenic microorganisms with the intestinal mucosal barrier. *Nat. Rev. Microbiol.* **16**, 457–470 (2018).
- Shan, M. et al. Mucus enhances gut homeostasis and oral tolerance by delivering immunoregulatory signals. *Science* **342**, 447–453 (2013).
- Parrish, A., Boudaud, M., Kuehn, A., Ollert, M. & Desai, M. S. Intestinal mucus barrier: a missing piece of the puzzle in food allergy. *Trends Mol. Med.* <https://doi.org/10.1016/j.molmed.2021.10.004> (2021).
- Desai, M. S. et al. A dietary fiber-deprived gut microbiota degrades the colonic mucus barrier and enhances pathogen susceptibility. *Cell* **167**, 1339–1353.e21 (2016).
- Earle, K. A. et al. Quantitative imaging of gut microbiota spatial organization. *Cell Host Microbe* <https://doi.org/10.1016/j.chom.2015.09.002> (2015).
- Schroeder, B. O. et al. Bifidobacteria or fiber protects against diet-induced microbiota-mediated colonic mucus deterioration. *Cell Host Microbe* **23**, 27–40 (2018).
- Neumann, M. et al. Deprivation of dietary fiber in specific-pathogen-free mice promotes susceptibility to the intestinal mucosal pathogen *Citrobacter rodentium*. *Gut Microbes* <https://doi.org/10.1080/19490976.2021.1966263> (2021).
- Loy, A. et al. Lifestyle and horizontal gene transfer-mediated evolution of *Mucispirillum schaedleri*, a core member of the murine gut microbiota. *mSystems* <https://doi.org/10.1128/msystems.00171-16> (2017).
- Pudlo, N. A. et al. Phenotypic and genomic diversification in complex carbohydrate-degrading human gut bacteria. *mSystems* <https://doi.org/10.1128/msystems.00947-21> (2022).
- Gustafsson, J. K. et al. An ex vivo method for studying mucus formation, properties, and thickness in human colonic biopsies and mouse small and large intestinal explants. *Am. J. Physiol. Gastrointest. Liver Physiol.* <https://doi.org/10.1152/ajpgi.00405.2011> (2012).
- Fort, M. M. et al. IL-25 induces IL-4, IL-5, and IL-13 and Th2-associated pathologies in vivo. *Immunity* [https://doi.org/10.1016/s1074-7613\(01\)00243-6](https://doi.org/10.1016/s1074-7613(01)00243-6) (2001).
- Parrish, A. et al. Dietary fibers boost gut microbiota-produced B vitamin pool and alter host immune landscape. Preprint at Res. Square <https://doi.org/10.21203/rs.3.rs-1563674/v2> (2022).
- Ganeshan, K. et al. Impairing oral tolerance promotes allergy and anaphylaxis: a new murine food allergy model. *J. Allergy Clin. Immunol.* **123**, 231–238.e4 (2009).
- Yu, W. et al. Allergen-specific CD8+ T cells in peanut-allergic individuals. *J. Allergy Clin. Immunol.* <https://doi.org/10.1016/j.jaci.2019.01.011> (2019).
- De Filippis, F. et al. Specific gut microbiome signatures and the associated pro-inflammatory functions are linked to pediatric allergy and acquisition of immune tolerance. *Nat. Commun.* <https://doi.org/10.1038/s41467-021-26266-z> (2021).
- Bell, A. et al. Elucidation of a sialic acid metabolism pathway in mucus-foraging *Ruminococcus gnavus* unravels mechanisms of bacterial adaptation to the gut. *Nat. Microbiol.* **4**, 2393–2404 (2019).
- Michalovich, D. et al. Obesity and disease severity magnify disturbed microbiome-immune interactions in asthma patients. *Nat. Commun.* **10**, 5711 (2019).
- Abdel-Gadir, A. et al. Microbiota therapy acts via a regulatory T cell MyD88/ROR γ pathway to suppress food allergy. *Nat. Med.* **25**, 1164–1174 (2019).
- Steimle, A. et al. Gut microbiome-based prediction of autoimmune neuroinflammation. Preprint at bioRxiv <https://doi.org/10.1101/2023.04.14.536901> (2023).
- Coleman, J. W., Buckley, M. G., Holliday, M. R. & Morris, A. G. Interferon- γ inhibits serotonin release from mouse peritoneal mast cells. *Eur. J. Immunol.* **21**, 2559–2564 (1991).
- Tkaczyk, C., Villa, I., Peronet, R., David, B. & Mécheri, S. Fc ϵ RI-mediated antigen endocytosis turns interferon- γ -treated mouse mast cells from inefficient into potent antigen-presenting cells. *Immunology* **97**, 333–340 (1999).
- Lacy, P., Logan, M. R., Bablitz, B. & Moqbel, R. Fusion protein vesicle-associated membrane protein 2 is implicated in IFN- γ -induced piecemeal degranulation in human eosinophils from atopic individuals. *J. Allergy Clin. Immunol.* **107**, 671–678 (2001).
- Chelakkot, C. et al. *Akkermansia muciniphila*-derived extracellular vesicles influence gut permeability through the regulation of tight junctions. *Exp. Mol. Med.* <https://doi.org/10.1038/emm.2017.282> (2018).
- Everard, A. et al. Cross-talk between *Akkermansia muciniphila* and intestinal epithelium controls diet-induced obesity. *Proc. Natl Acad. Sci. USA* **110**, 9066–9071 (2013).
- Ansaldo, E. et al. *Akkermansia muciniphila* induces intestinal adaptive immune responses during homeostasis. *Science* **364**, 1179–1184 (2019).
- Cani, P. D., Depommier, C., Derrien, M., Everard, A. & de Vos, W. M. *Akkermansia muciniphila*: paradigm for next-generation beneficial microorganisms. *Nat. Rev. Gastroenterol. Hepatol.* **19**, 625–637 (2022).

37. Rodrigues, V. F. et al. *Akkermansia muciniphila* and gut immune system: a good friendship that attenuates inflammatory bowel disease, obesity, and diabetes. *Front. Immunol.* **13**, 934695 (2022).
38. Derrien, M. et al. Modulation of mucosal immune response, tolerance, and proliferation in mice colonized by the mucin-degrader *Akkermansia muciniphila*. *Front. Microbiol.* <https://doi.org/10.3389/fmicb.2011.00166> (2011).
39. Hadis, U. et al. Intestinal tolerance requires gut homing and expansion of FoxP3+ regulatory T cells in the lamina propria. *Immunity* **34**, 237–246 (2011).
40. Knoop, K. A., McDonald, K. G., McCrate, S., McDole, J. R. & Newberry, R. D. Microbial sensing by goblet cells controls immune surveillance of luminal antigens in the colon. *Mucosal Immunol.* <https://doi.org/10.1038/mi.2014.58> (2015).
41. Aguilera-Lizarraga, J. et al. Local immune response to food antigens drives meal-induced abdominal pain. *Nature* <https://doi.org/10.1038/s41586-020-03118-2> (2021).
42. Wasielewska, Z., Dolińska, A., Wilczyńska, D., Szaflarska-Popławska, A. & Krogulska, A. Prevalence of allergic diseases in children with inflammatory bowel disease. *Postepy Dermatol. Alergol.* **36**, 286–294 (2019).
43. Cai, C. et al. Serological investigation of food specific immunoglobulin G antibodies in patients with inflammatory bowel diseases. *PLoS ONE* **9**, e112154 (2014).
44. Guilarte, M. et al. Diarrhoea-predominant IBS patients show mast cell activation and hyperplasia in the jejunum. *Gut* <https://doi.org/10.1136/gut.2006.100594> (2007).
45. Tsoi, L. C. et al. Progression of acute-to-chronic atopic dermatitis is associated with quantitative rather than qualitative changes in cytokine responses. *J. Allergy Clin. Immunol.* **145**, 1406–1415 (2020).
46. Gittler, J. K. et al. Progressive activation of TH2/TH22 cytokines and selective epidermal proteins characterizes acute and chronic atopic dermatitis. *J. Allergy Clin. Immunol.* **130**, 1344–1354 (2012).
47. Connors, L., O’Keefe, A., Rosenfield, L. & Kim, H. Non-IgE-mediated food hypersensitivity. *Allergy Asthma Clin. Immunol.* **14**, 56 (2018).
48. Steimle, A. et al. Constructing a gnotobiotic mouse model with a synthetic human gut microbiome to study host–microbe cross talk. *STAR Protoc.* <https://doi.org/10.1016/j.xpro.2021.100607> (2021).
49. Kozich, J. J., Westcott, S. L., Baxter, N. T., Highlander, S. K. & Schloss, P. D. Development of a dual-index sequencing strategy and curation pipeline for analyzing amplicon sequence data on the MiSeq illumina sequencing platform. *Appl. Environ. Microbiol.* <https://doi.org/10.1128/aem.01043-13> (2013).
50. Bolyen, E. et al. Reproducible, interactive, scalable and extensible microbiome data science using QIIME 2. *Nat. Biotechnol.* <https://doi.org/10.1038/s41587-019-0209-9> (2019).
51. Quast, C. et al. The SILVA ribosomal RNA gene database project: improved data processing and web-based tools. *Nucleic Acids Res.* <https://doi.org/10.1093/nar/gks1219> (2013).
52. Oksanen, J. et al. Package ‘vegan’: Community Ecology Package (CRAN, 2019).
53. Martínez Arbizu, P. pairwiseAdonis: Pairwise Multilevel Comparison Using Adonis. R package v0.4. (GitHub, 2020).
54. McMurdie, P. J. & Holmes, S. Phyloseq: an R package for reproducible interactive analysis and graphics of microbiome census data. *PLoS ONE* <https://doi.org/10.1371/journal.pone.0061217> (2013).
55. Wickham, H. *Package ‘ggplot2’: Elegant Graphics for Data Analysis* (Springer, 2016).
56. Love, M. I., Huber, W. & Anders, S. Moderated estimation of fold change and dispersion for RNA-seq data with DESeq2. *Genome Biol.* <https://doi.org/10.1186/s13059-014-0550-8> (2014).
57. Nowicka, M. et al. CyTOF workflow: differential discovery in high-throughput high-dimensional cytometry datasets. *F1000Research* <https://doi.org/10.12688/f1000research.11622.3> (2019).
58. Leonard, C. et al. Comprehensive mapping of immune tolerance yields a regulatory TNF receptor 2 signature in a murine model of successful Fel d 1-specific immunotherapy using high-dose CpG adjuvant. *Allergy* <https://doi.org/10.1111/all.14716> (2021).
59. Van Gassen, S. et al. FlowSOM: using self-organizing maps for visualization and interpretation of cytometry data. *Cytometry A* <https://doi.org/10.1002/cyto.a.22625> (2015).
60. McInnes, L., Healy, J. & Melville, J. UMAP: Uniform Manifold Approximation and Projection for Dimension Reduction. *arXiv* <https://doi.org/10.48550/arXiv.1802.03426> (2020).
61. Greenhalgh, K. et al. Integrated in vitro and *in silico* modeling delineates the molecular effects of a symbiotic regimen on colorectal-cancer-derived cells. *Cell Rep.* <https://doi.org/10.1016/j.celrep.2019.04.001> (2019).
62. Steimle, A., Grant, E. T. & Desai, M. S. Quantitative assay to detect bacterial glycan-degrading enzyme activities in mouse and human fecal samples. *STAR Protoc.* <https://doi.org/10.1016/j.xpro.2021.100326> (2021).

Acknowledgements

M.S.D. was supported by the Luxembourg National Research Fund (FNR) CORE grants (C15/BM/10318186 and C18/BM/12585940) and BRIDGES grant (22/17426243); A.P. was supported by an FNR AFR individual PhD fellowship (11602973); M.B. was supported by a European Commission Horizon 2020 Marie Skłodowska-Curie Actions individual fellowship (897408); E.T.G. was supported by FNR PRIDE (17/11823097) and the Fondation du Pélican de Mie et Pierre Hippert-Faber, under the aegis of the Fondation de Luxembourg; S.Z.C. was supported by FNR PRIDE (19/14254520); and M.N. was supported by the FNR AFR bilateral grant (15/11228353). We thank MEDICE Arzneimittel Pütter GmbH & Co. KG, Germany and Theralution GmbH, Germany for funding through the public–private partnership FNR BRIDGES grant (22/17426243); the National Cytometry Platform (NCP); and the Cytométrie Pitié-Salpêtrière (CyPS) for their assistance with generating cytometry data. The NCP is supported by Luxembourg’s Ministry of Higher Education and Research (MESR) funding. We also acknowledge the support of C. Jäger, X. Dong and F. Gavotto from the Luxembourg Centre for Systems Biomedicine (LCSB) Metabolomics Platform for GC-MS analyses; G. Hansson and G. Birchenough (University of Gothenburg, Sweden) for helping us set up the assay for measuring mucus penetrability. For the purpose of open access, and in fulfilment of the obligations arising from the grant agreement, the authors have applied for a Creative Commons Attribution 4.0 International (CC BY 4.0) licence to any author-accepted paper version arising from this submission.

Author contributions

M.S.D. supervised the research and obtained research funding. A.P., M.B., M.O., and M.S.D. conceived the research. A.P., M.B. and M.S.D. designed the experiments. A.P. and S.W. performed the experiments, and A.P. and M.B. analysed the data. M.N., M.W. and S.Z.C. assisted with mucus layer staining and measurements. A.D.S. assisted with germ-free animal experiments and beads assay and performed qPCR analyses. E.T.G. performed enzyme assay experiments and analysed the 16S rRNA gene sequencing data. A.C. helped with CyTOF experiments. O.H. performed the CyTOF data analysis. A.P., M.B. and M.S.D. wrote the paper. All authors reviewed and edited the paper.

Competing interests

M.S.D. works as a consultant and an advisory board member at Theralution GmbH, Germany. All other authors declare no competing interests.

Additional information

Extended data is available for this paper at
<https://doi.org/10.1038/s41564-023-01464-1>.

Supplementary information The online version contains supplementary material available at
<https://doi.org/10.1038/s41564-023-01464-1>.

Correspondence and requests for materials should be addressed to Mahesh S. Desai.

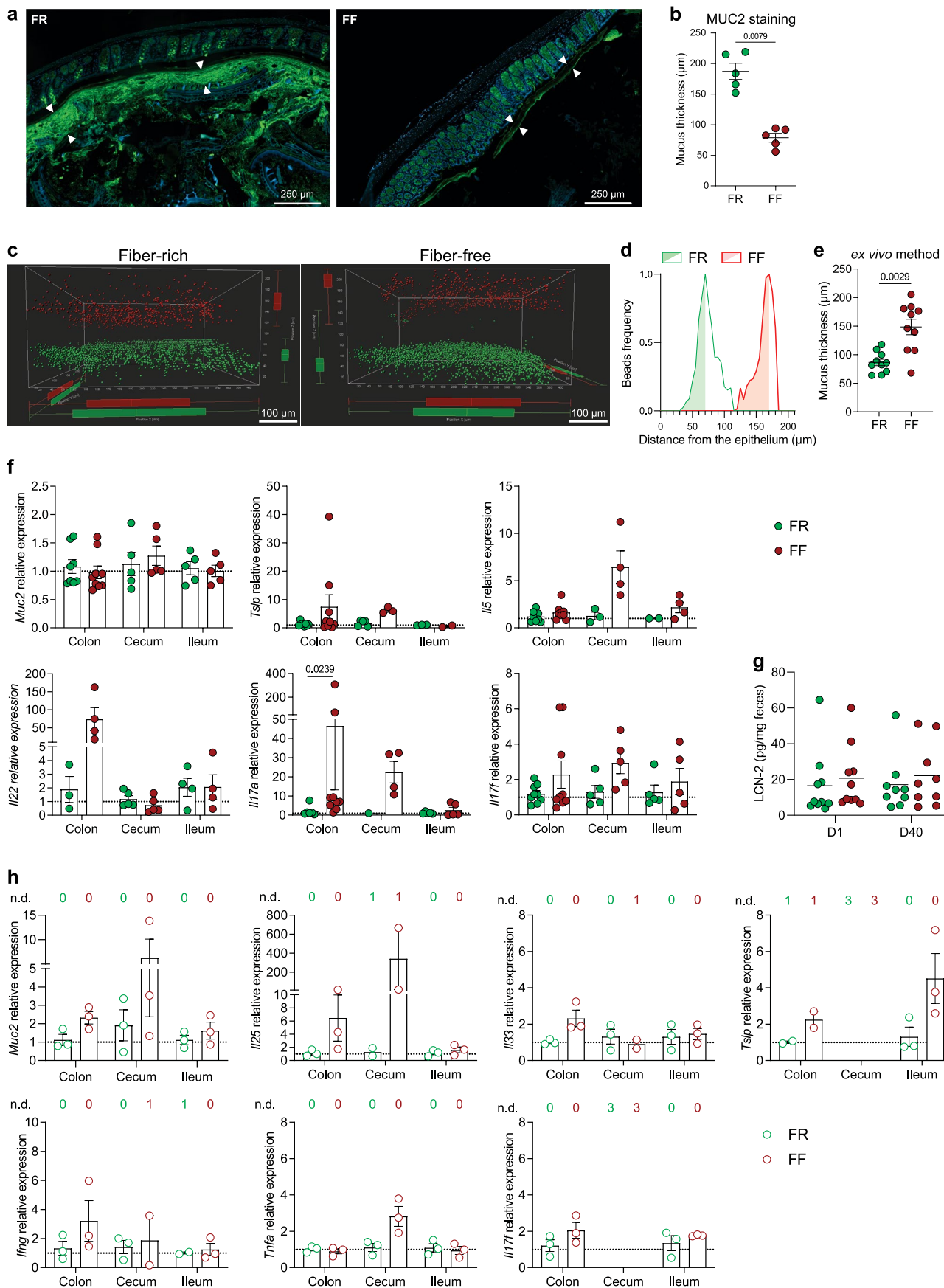
Peer review information *Nature Microbiology* thanks Elena Verdu and the other, anonymous, reviewer(s) for their contribution to the peer review of this work.

Reprints and permissions information is available at
www.nature.com/reprints.

Publisher's note Springer Nature remains neutral with regard to jurisdictional claims in published maps and institutional affiliations.

Open Access This article is licensed under a Creative Commons Attribution 4.0 International License, which permits use, sharing, adaptation, distribution and reproduction in any medium or format, as long as you give appropriate credit to the original author(s) and the source, provide a link to the Creative Commons license, and indicate if changes were made. The images or other third party material in this article are included in the article's Creative Commons license, unless indicated otherwise in a credit line to the material. If material is not included in the article's Creative Commons license and your intended use is not permitted by statutory regulation or exceeds the permitted use, you will need to obtain permission directly from the copyright holder. To view a copy of this license, visit <http://creativecommons.org/licenses/by/4.0/>.

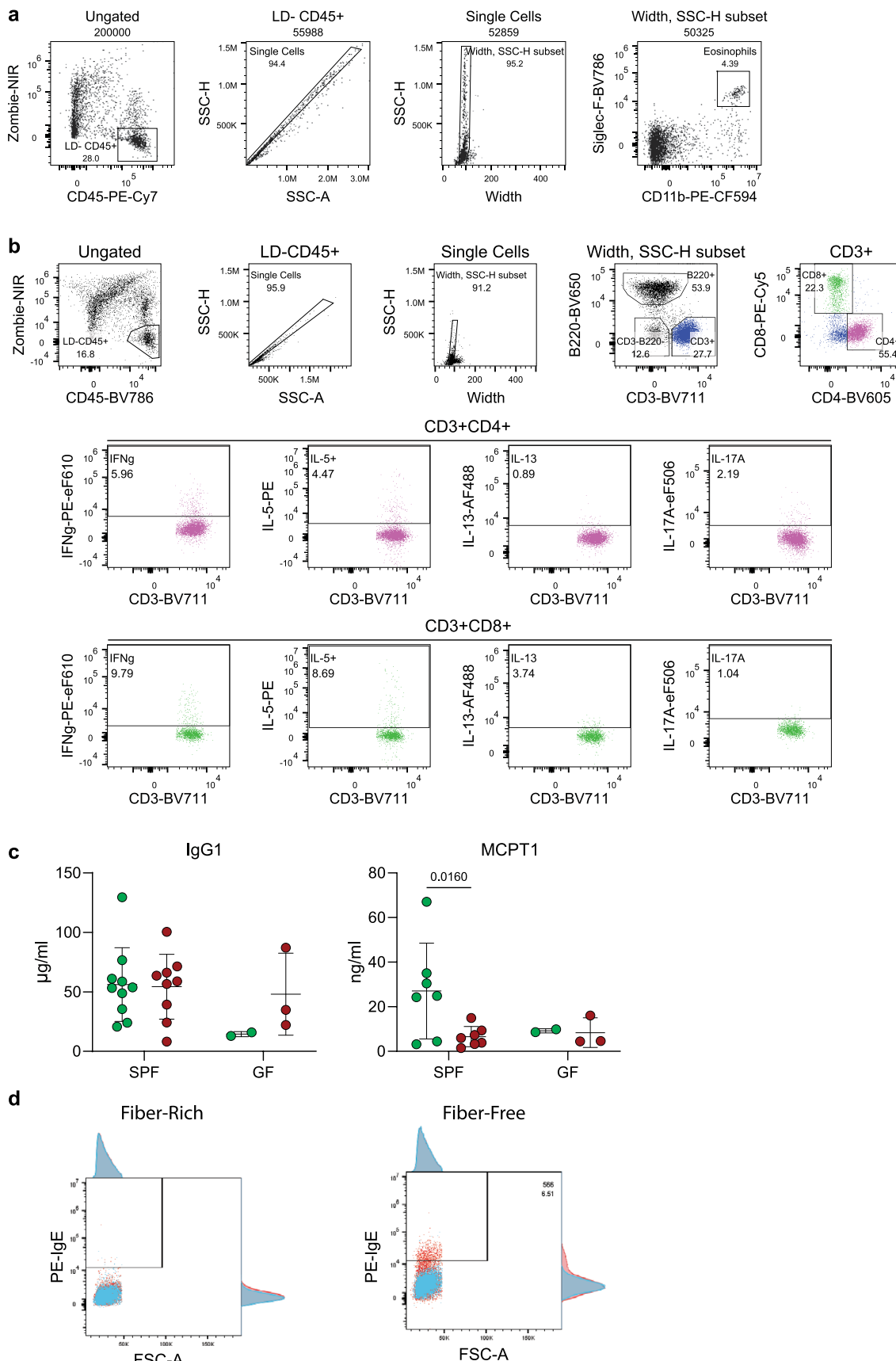
© The Author(s) 2023



Extended Data Fig. 1 | See next page for caption.

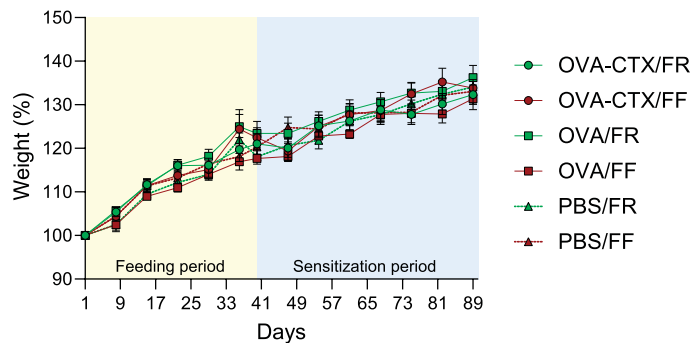
Extended Data Fig. 1 **a**, Representative immunofluorescence images of distal colon sections stained with α -Muc2 (green) and DAPI (blue). White arrow heads indicate the edges of the mucus layer. **b**, Mucus thickness measured on colonic section stained with α -Muc2. Each dot is the average of several measurements from one animal ($n = 5$ mice per group, two-tailed Mann-Whitney test). **c**, Representative images of distal colonic tissues showing 1- μm -sized beads (red dots) laying on top of the epithelium (green dots) using an *ex situ ex vivo* method. The space between the beads and the epithelium exemplify the unpenetrable mucus layer. **d**, Analysis of the images presented in b showing the frequency of beads as a function of the distance of the epithelium for the FR-fed (green line) and the FF-fed (red line) sample. The penetration of the beads into the mucus is represented and quantified as the area under the curve to the peak (colored area under the curve). **e**, Colonic mucus thickness measured *ex vivo* as the distance of 1- μm -sized beads peak from the epithelium (as shown in d). Each dot is the

average of 4–7 measurements from one animal ($n = 10$ mice per group, two-tailed Mann-Whitney test). **f**, Relative transcript levels of *Muc2*, *Tslp*, *Il5*, *Il22*, *Il17a* and *Il17f* in the colon, cecum, and ileum of SPF mice fed a FR (green) or a FF (red) diet. Expression levels were normalized to the FR group, independently for each tissue ($n = 5$ –10 mice per group, two independent experiments, multiple Mann-Whitney test, P values adjusted using the Benjamini-Hochberg method). **g**, Fecal lipocalin-2 (LCN-2) measured at the beginning (D1) and at the end (D40) of the 40-day feeding period ($n = 9$ –10). **h**, Relative transcript levels of selected cytokine mRNA in the colon, cecum and ileum of germfree mice. Transcript levels were normalized to the FR group, independently for each tissue. Numbers above dot plots represent the number of samples in which transcripts were not detected (n.d.) ($n = 3$ mice per group). All dot plots are represented with mean \pm SEM.

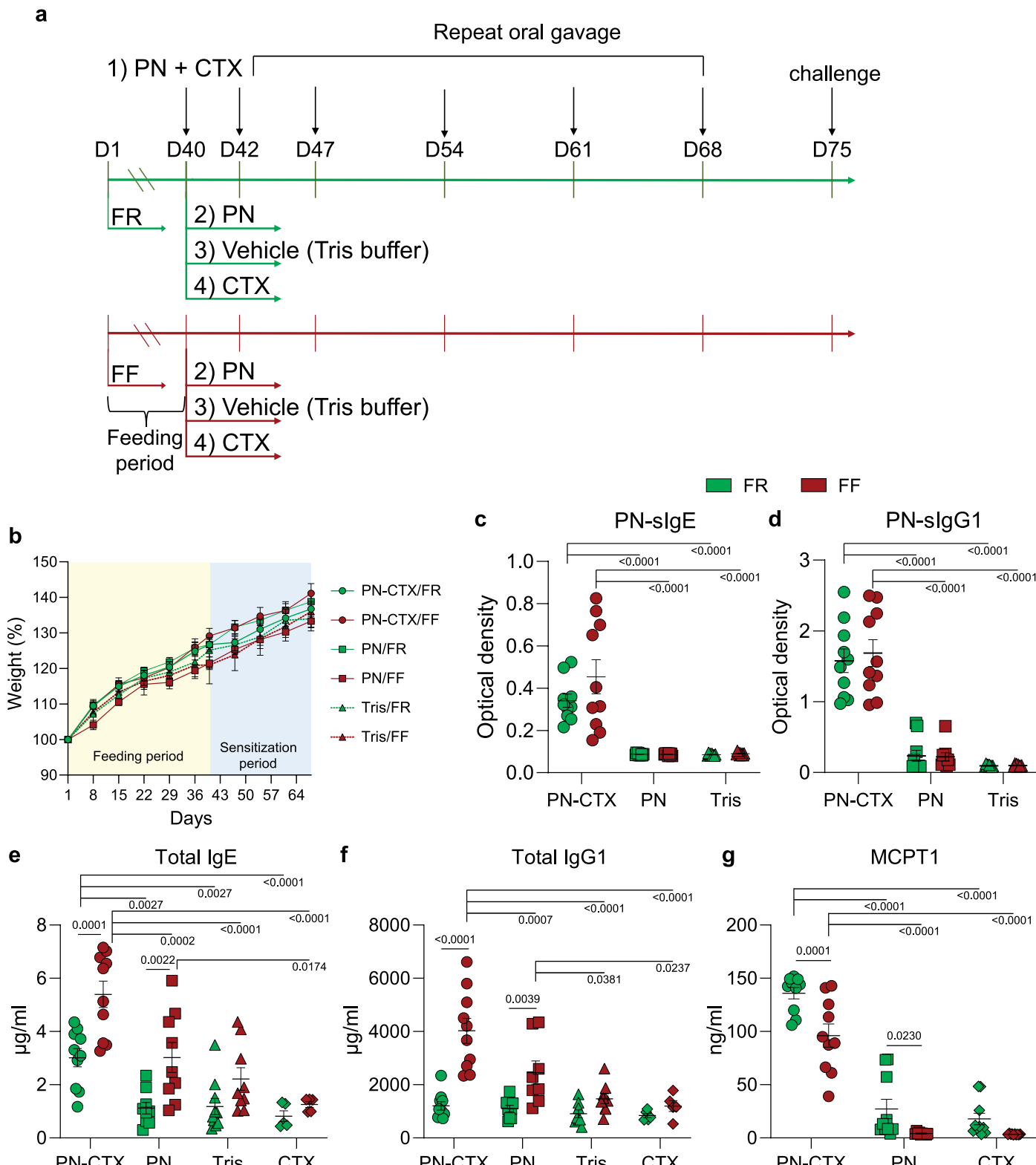


Extended Data Fig. 2 **a**, Gating strategy for eosinophils, defined as Siglec-F⁺CD11b⁺ singlets. **b**, Gating strategy for cytokine-expressing CD4⁺ and CD8⁺ T lymphocytes. **c**, Serum titers of IgG1 and mouse mucosal mast cell protease 1 (MCPT1) ($n = 2-10$, two-way ANOVA, P values adjusted using the Benjamini-

Hochberg method). **d**, Representative plots for IgE-coated bacteria in fiber-rich and fiber-free fed mice. Each sample was stained with an α -IgE antibody (red) or an isotype control (blue).

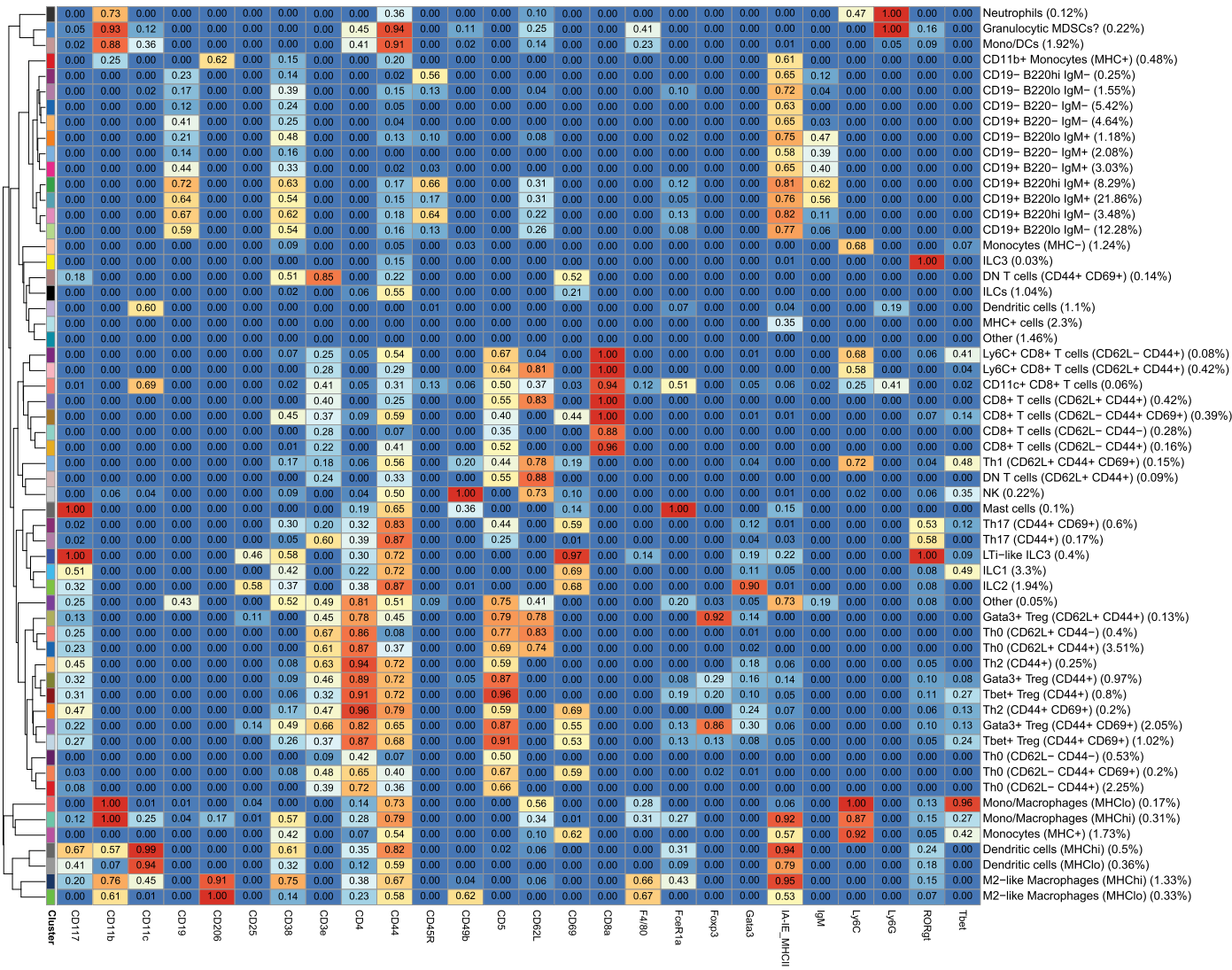


Extended Data Fig. 3 | Weight curves of the mice over the 40-day feeding period and the sensitization period to OVA-CTX ($n = 5\text{--}10$, mixed-effects model with matched values per mice, time effect $P < 0.0001$).

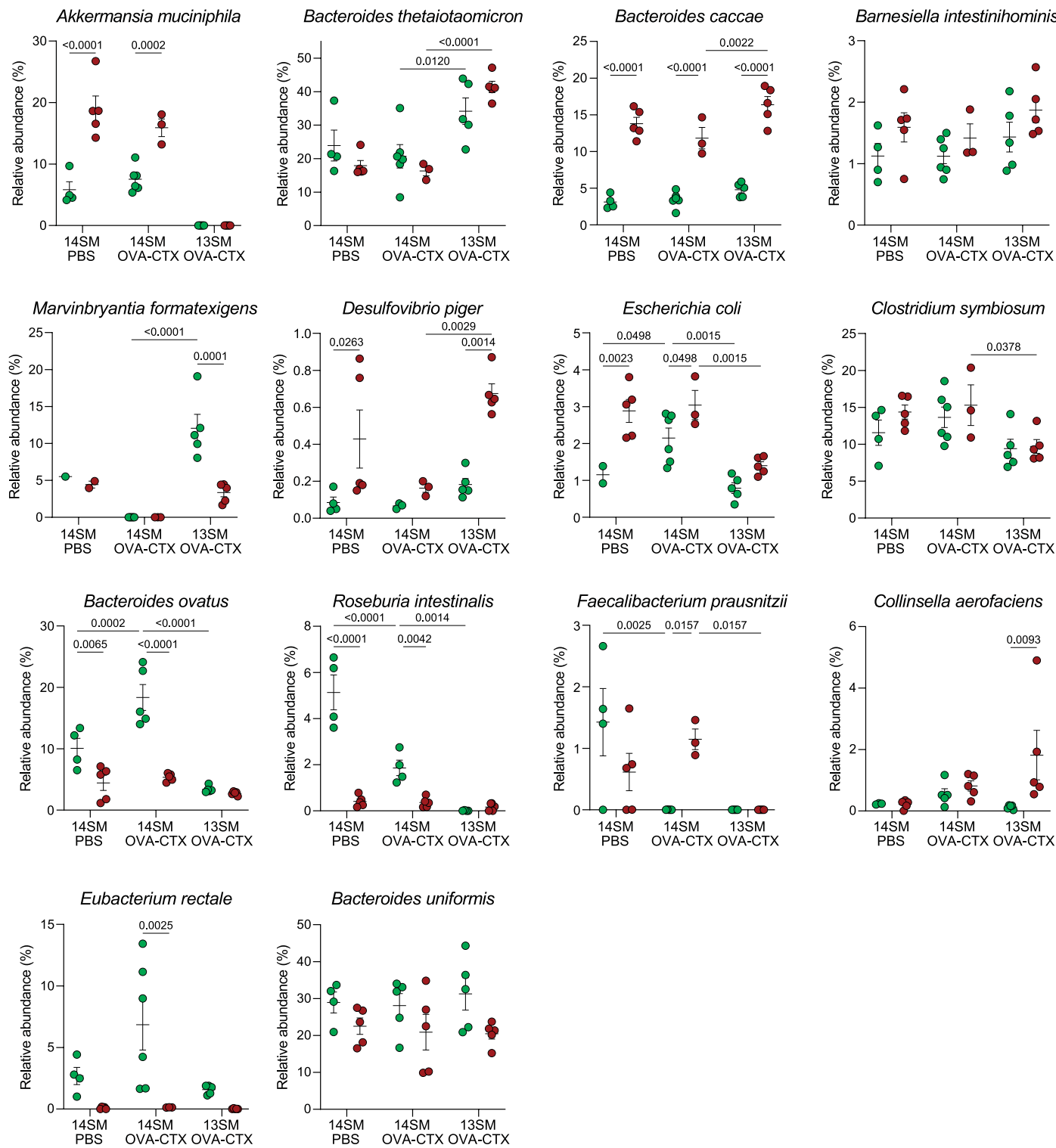


Extended Data Fig. 4 |a, Schematic timeline for peanut protein (PN) sensitization with cholera toxin (CTX) as an adjuvant and control groups. Samples were collected 3 h after the challenge. **b**, Weight curves of the mice over the 40-day feeding period and the sensitization period to PN-CTX ($n=10$, two independent experiments, mixed-effects model with matched values per

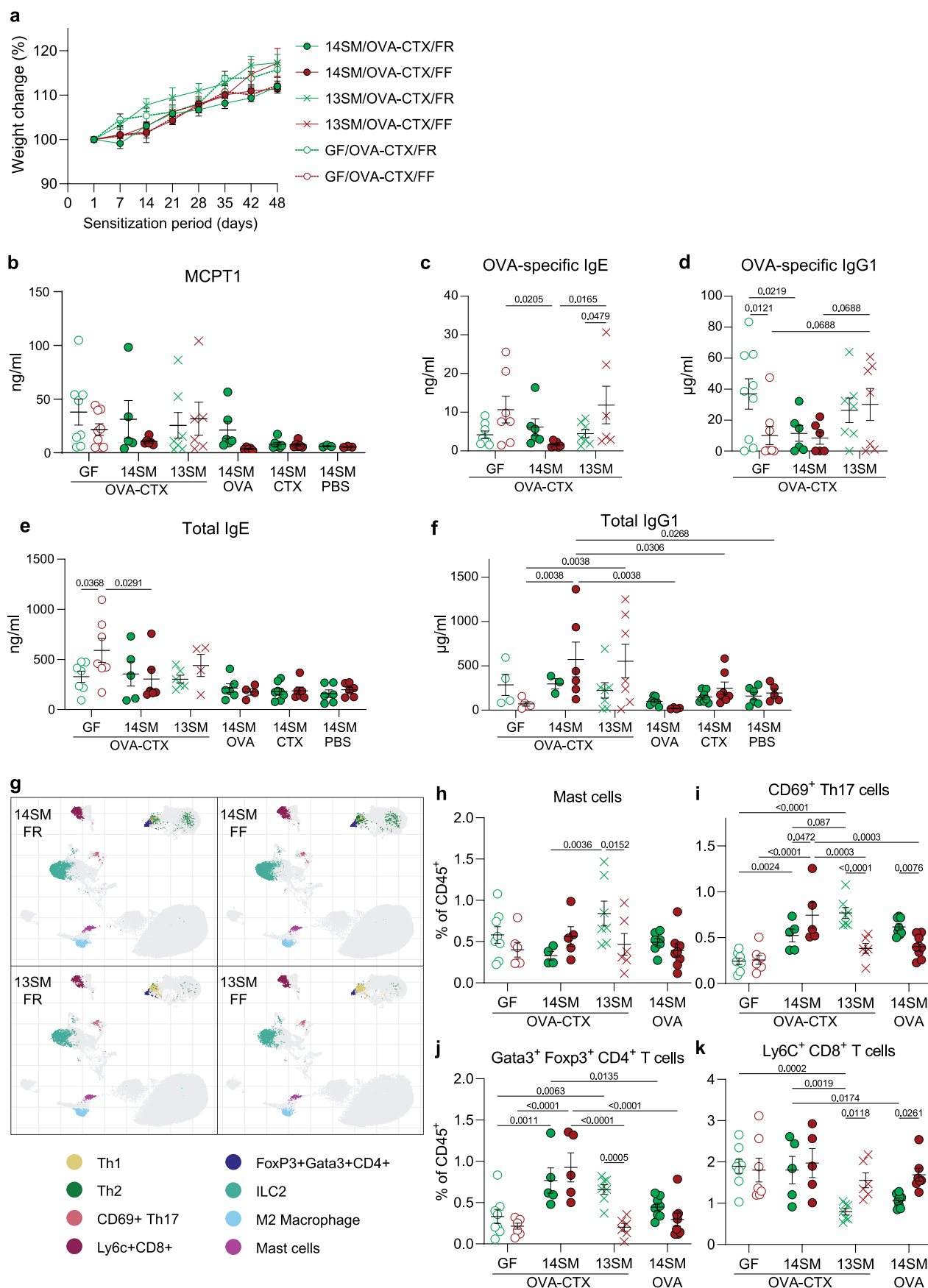
mice, time effect $P<0.0001$). **c-g**, Serum titers of PN-specific IgE (**c**, $n=9-10$), PN-specific IgG1 (**d**, $n=9-10$), total IgE (**e**, $n=5-10$), total IgG1 (**f**, $n=5-10$), and mouse mast cell protease 1 (**g**, MCPT1, $n=10$). Two-way ANOVA, P values adjusted using the Benjamini-Hochberg method. Fiber-rich (FR, green), fiber-free (FF, red). All dot plots are represented with mean \pm SEM.



Extended Data Fig. 5 | Heatmap of the 58 annotated clusters identified by FlowSOM from CyTOF analysis of colonic lamina propria cells of SPF mice 24 h after challenge. Numbers in the heatmap indicate the relative expression of each marker among cell populations. Percentages shown in parentheses represent frequencies of populations among CD45⁺ cells.



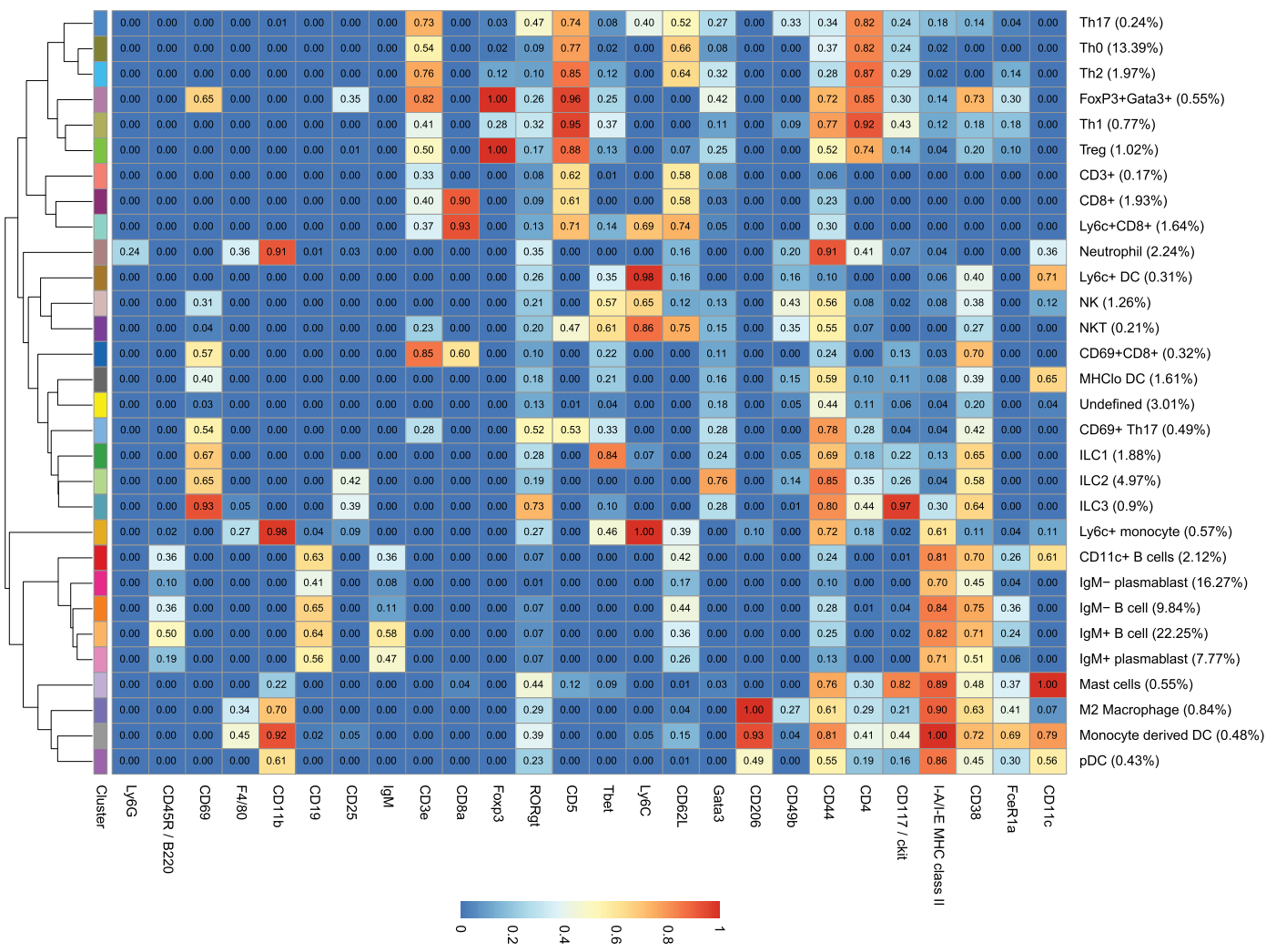
Extended Data Fig. 6 | Relative abundances of indicated bacterial strains from feces of FR-fed (green) and FF-fed (red) mice, at the end of the experiment ($n = 3–6$, two-way ANOVA, P values adjusted using the Benjamini-Hochberg method). All dot plots are represented with mean \pm SEM.



Extended Data Fig. 7 | See next page for caption.

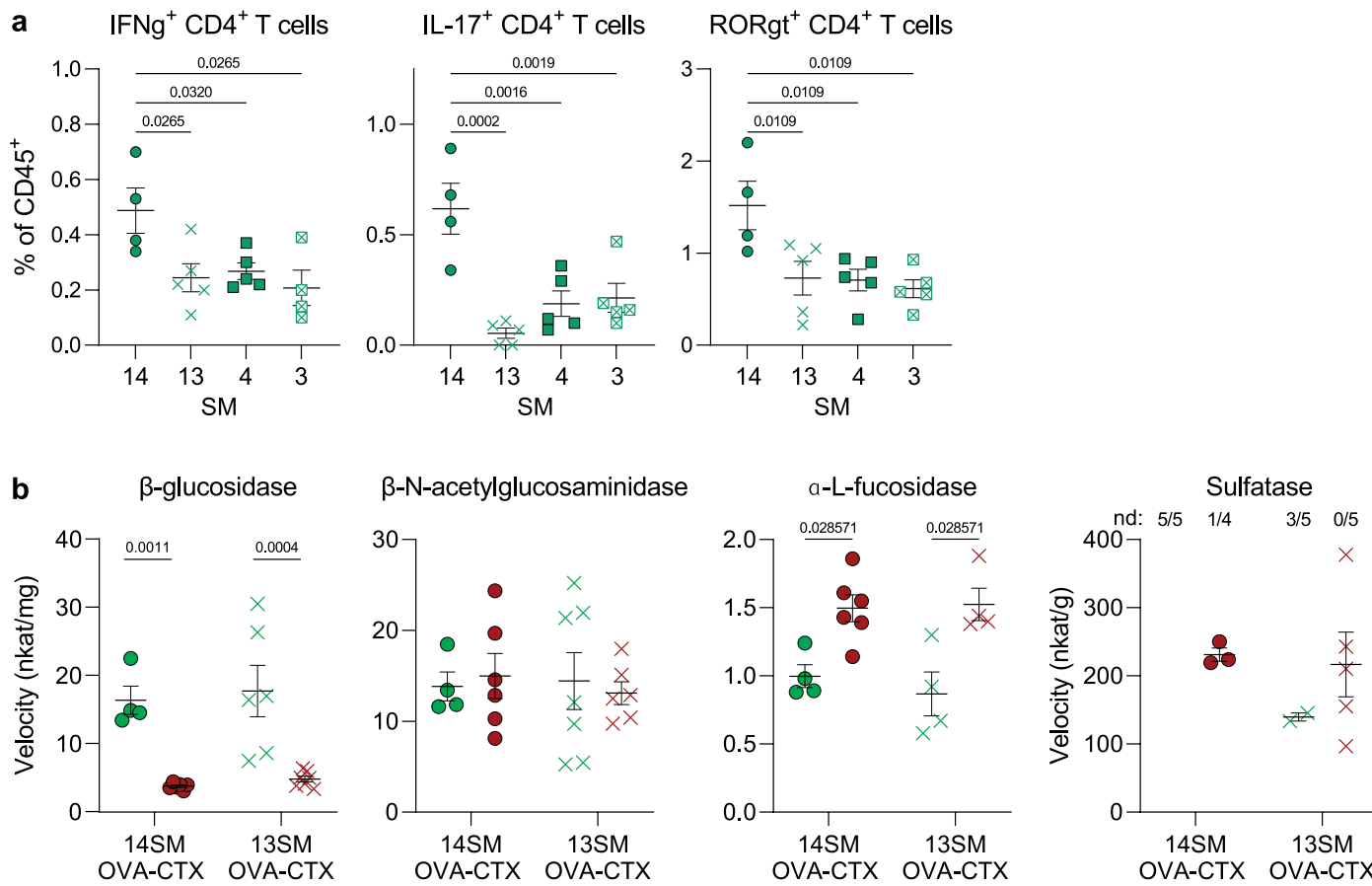
Extended Data Fig. 7 | a, Weight curves of the mice over the sensitization period to OVA-CTX ($n = 3–9$, two-way ANOVA with matched values per mice, time effect $P < 0.0001$). **b–f**, Serum titers of MCPT1 (**b**), OVA-specific IgE (**c**), OVA-specific IgG1 (**d**), total IgE (**e**), and total IgG1 (**f**) ($n = 4–10$ mice per group, two independent experiments, two-way ANOVA, P values adjusted using the Benjamini-Hochberg method). Note that the serum titers of OVA-specific IgE and OVA-specific IgG1 were below the limit of detection in other groups.

g, Uniform manifold approximation and projection (UMAP) of specific populations identified using FlowSOM among CD45⁺ cells from the colonic lamina propria of OVA-CTX sensitized, 14SM- and 13SM-colonized mice 24 h after challenge. Highlighted populations are the ones showing differences between groups. **h–k**, Frequencies of indicated cell populations among cLP CD45⁺ cells ($n = 5–10$, two-way ANOVA, unadjusted P values, non-significant after adjustment using the Benjamini-Hochberg method).



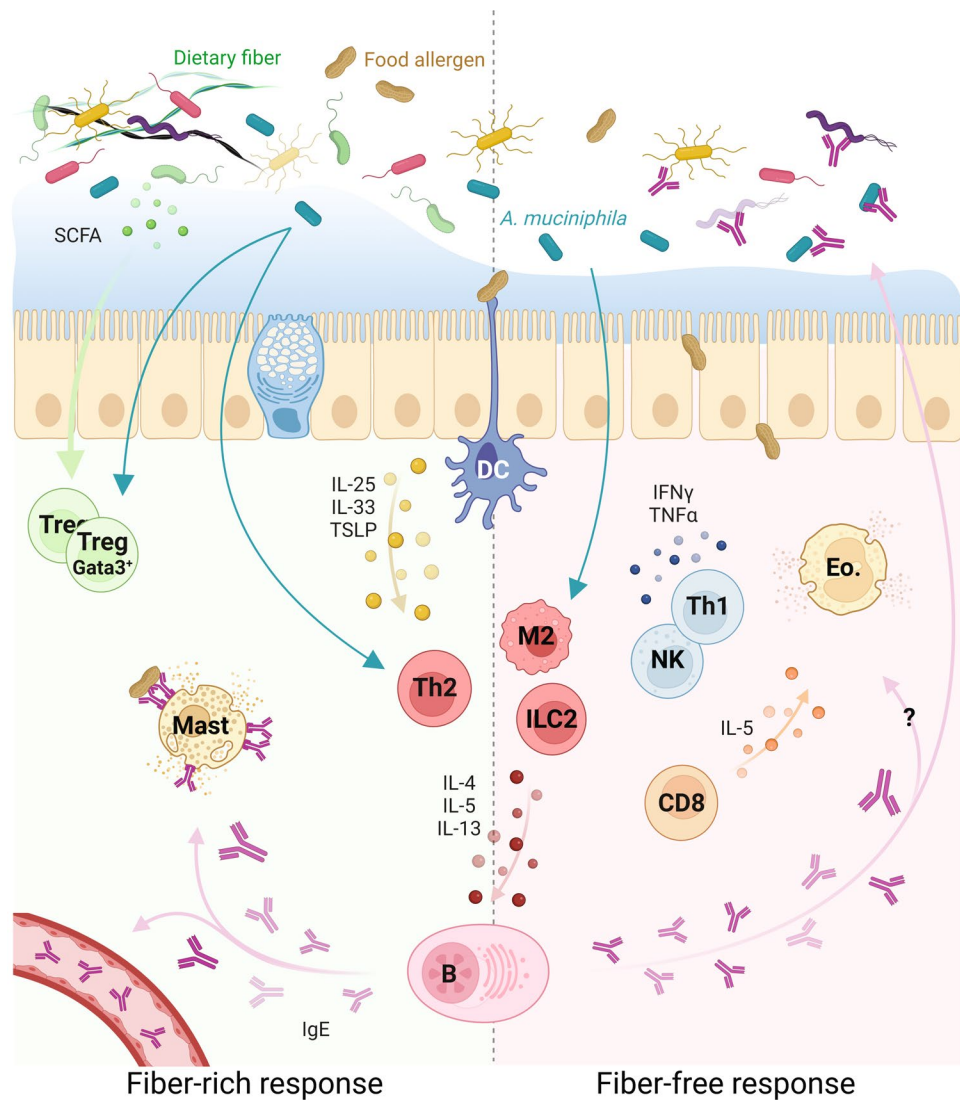
Extended Data Fig. 8 | Heatmap of the 30 annotated clusters identified by FlowSOM from CyTOF analysis of colonic lamina propria cells of GF and gnotobiotic OVA-sensitized mice 24 h after challenge. Numbers in the

heatmaps indicate the relative expression of each marker among cell populations. Percentages shown in parentheses represent frequencies of populations among CD45⁺ cells. All dot plots are represented with mean +/− SEM.



Extended Data Fig. 9 | a. A figure panel from previously published data by Steinle et al.²⁹, showing proportions of indicated cell populations among CD45⁺ cells in the colonic lamina propria of mice colonized with 3SM (*B. caccae*, *B. thetaiotaomicron*, *B. intestinalis*), 4SM (3SM + *A. muciniphila*), 13SM (3SM + 10 non-mucin-degrading bacteria) or 14SM (13SM + *A. muciniphila*) ($n = 4-5$, one-way ANOVA, P values adjusted using the Benjamini-Hochberg

b. Enzymatic activity of select carbohydrate-active enzymes (CAZymes) and sulfatase measured in the feces of OVA-CTX-sensitized, 14SM- and 13SM-colonized mice ($n = 4-7$, multiple Mann-Whitney, P values adjusted using the Benjamini-Hochberg method). Fiber-rich (green), fiber-free (red). All dot plots are represented with mean \pm SEM.


Extended Data Fig. 10 | Proposed model of colonic immune pathways during an allergic response under a fiber-rich (left) versus a fiber-free (right) diet.

Allergic type-2 responses at the intestinal barrier are initiated by the sensing of the allergen and the release of epithelial-derived cytokines IL-25, IL-33 and TSLP that promote the recruitment and activation of type 2 immune cells Th2, M2 macrophages and ILC2, and lead to the production of IgE. Under a fiber-rich diet, Treg cells are maintained in response to microbiota-derived SCFAs, and *Akkermansia muciniphila* promotes Gata3⁺ Treg cells as well as Th2 cells. In this context, a conventional allergic response is driven by IgE-primed mast cell degranulation. By contrast, fiber deprivation leads to a non-canonical allergy response driven by the altered microbiota composition and the increased intestinal permeability, which altogether predisposes to a mixed inflammatory

environment comprising of innate type 2 cells, M2 and ILC2, and type 1 cells, Th1, NK and CD8⁺ T cells. In this context, an allergic response is characterized by the production of IL-5 that is reinforced by CD8⁺ T cells and mediates eosinophilia. This chain of events is paralleled by higher coating of colonic bacteria by IgE, which has an unknown role in the pathology. The fiber deprivation-induced mucus changes and increased intestinal permeability are likely to facilitate the microbiota-driven type 1 responses, but further studies are needed to determine their contribution to the innate type 2 response that is promoted by *A. muciniphila*. Finally, the role of intestinal IgEs and their antigenic specificity in the eosinophilic reaction remain an important question to address in the future. Created with BioRender.com.

Corresponding author(s): Mahesh S Desai

Last updated by author(s): Jul 26, 2023

Reporting Summary

Nature Portfolio wishes to improve the reproducibility of the work that we publish. This form provides structure for consistency and transparency in reporting. For further information on Nature Portfolio policies, see our [Editorial Policies](#) and the [Editorial Policy Checklist](#).

Statistics

For all statistical analyses, confirm that the following items are present in the figure legend, table legend, main text, or Methods section.

n/a Confirmed

- The exact sample size (n) for each experimental group/condition, given as a discrete number and unit of measurement
- A statement on whether measurements were taken from distinct samples or whether the same sample was measured repeatedly
- The statistical test(s) used AND whether they are one- or two-sided
Only common tests should be described solely by name; describe more complex techniques in the Methods section.
- A description of all covariates tested
- A description of any assumptions or corrections, such as tests of normality and adjustment for multiple comparisons
- A full description of the statistical parameters including central tendency (e.g. means) or other basic estimates (e.g. regression coefficient) AND variation (e.g. standard deviation) or associated estimates of uncertainty (e.g. confidence intervals)
- For null hypothesis testing, the test statistic (e.g. F , t , r) with confidence intervals, effect sizes, degrees of freedom and P value noted
Give P values as exact values whenever suitable.
- For Bayesian analysis, information on the choice of priors and Markov chain Monte Carlo settings
- For hierarchical and complex designs, identification of the appropriate level for tests and full reporting of outcomes
- Estimates of effect sizes (e.g. Cohen's d , Pearson's r), indicating how they were calculated

Our web collection on [statistics for biologists](#) contains articles on many of the points above.

Software and code

Policy information about [availability of computer code](#)

Data collection No custom software was used for data collection.

Data analysis

No custom algorithms or software were used for data analysis. The analysis pipelines in this study employ tools that have been previously described in published literature and are described below. The code used to analyze these data can be found at <https://github.com/DII-LIH-Luxembourg>.

Mass cytometry data analysis: Each organ was analyzed independently following the same analysis pipeline, as previously described by Leonard et al (doi:10.1111/all.14716.). FCS files were normalized with the normalization passport EQ-P13H2303_ver2. FCS files were uploaded into FlowJo™ software version 10.8.1 for cleaning. Unsupervised analysis was carried out in RStudio (version 1.0.143, R version 3.4.4) using the R package ‘flowcore’ version 1.44.2. Single cells were clustered using FlowSOM. Statistical analysis were performed using GraphPad Prism version 8.0.0 & 9.0.0 for Windows (GraphPad Software, San Diego, California USA, www.graphpad.com).

16S rRNA gene sequencing and analysis: Raw sequences were processed using QIIME2 version 2020.6 with DADA2 for sequence quality control and taxonomic assignment was performed using the “classify-consensus-vsearch” method against the SILVA 138 reference database. Further analyses were performed in R version 4.0.2 using the package ‘phyloseq’ version 1.34.0. PCoA plots were generated using the package ‘vegan’ version 2.5-7, with clustering significance testing using package ‘pairwiseAdonis’ version 0.4. Differential enrichment analysis was performed using the package ‘DESeq2’ version 1.30.1, which implements the Wald test to determine statistical significance (p value adjustment using Benjamini-Hochberg method). Visualizations were generated using ‘ggplot2’ version 3.3.5 and ‘forcats’ version 0.5.1.

Image analysis for mucus penetrability assay: Images were acquired with the software Zen3.0 (Blue Edition, Carl Zeiss Microscopy GmbH) and then analyzed with Imaris software (Oxford Instruments Imaris).

Goblet cell count: goblets cells per crypts were counted using the ImageJ software (<https://imagej.nih.gov/>).

For manuscripts utilizing custom algorithms or software that are central to the research but not yet described in published literature, software must be made available to editors and reviewers. We strongly encourage code deposition in a community repository (e.g. GitHub). See the Nature Portfolio [guidelines for submitting code & software](#) for further information.

Data

Policy information about [availability of data](#)

All manuscripts must include a [data availability statement](#). This statement should provide the following information, where applicable:

- Accession codes, unique identifiers, or web links for publicly available datasets
- A description of any restrictions on data availability
- For clinical datasets or third party data, please ensure that the statement adheres to our [policy](#)

The raw fastq files from 16S rRNA gene sequencing have been deposited in the European Nucleotide Archive (ENA) at EMBL-EBI under accession numbers PRJEB53451 (<https://www.ebi.ac.uk/ena/browser/view/PRJEB53451>) and PRJEB51707 (<https://www.ebi.ac.uk/ena/browser/view/PRJEB51707>). The mass cytometry datasets for colonic lamina propria have been uploaded to the FlowRepository database under accession number FR-FCM-Z5G2 (<https://flowrepository.org/>).

Field-specific reporting

Please select the one below that is the best fit for your research. If you are not sure, read the appropriate sections before making your selection.

Life sciences

Behavioural & social sciences

Ecological, evolutionary & environmental sciences

For a reference copy of the document with all sections, see nature.com/documents/nr-reporting-summary-flat.pdf

Life sciences study design

All studies must disclose on these points even when the disclosure is negative.

Sample size	Under the animal protocols, a minimum sample size of 5 mice per group was determined to be sufficient to have at least 90% power to detect statistically significant ($p<0.05$) changes in mucus layer thickness. As preliminary results were acquired, sample sizes were revised with the readouts of interest, ie. symptom scores at challenge and cytometry results. A sample size of 7 to 10 mice per group was finally approved to be sufficient to have at least 80% power to detect statistically significant ($p<0.05$) changes in symptom scores.
Data exclusions	In 16S gene sequencing analyses, taxa not observed more than once on average across all samples were removed and the data was rarefied to the minimum library size.
Replication	All experiments were reproduced at least twice in independent batches. We did not detect batch effects.
Randomization	Mice were housed in individual cages with up to 5 mice per cage. Each cage was assigned at random to one of the 2 dietary groups: fiber-rich or fiber-free.
Blinding	Symptom scoring was performed blinded by 2 independent experimenters to avoid subconscious researcher biases. All biological samples were processed and analyzed blindly regarding the experimental groups.

Reporting for specific materials, systems and methods

We require information from authors about some types of materials, experimental systems and methods used in many studies. Here, indicate whether each material, system or method listed is relevant to your study. If you are not sure if a list item applies to your research, read the appropriate section before selecting a response.

Materials & experimental systems

n/a	Involved in the study
<input type="checkbox"/>	<input checked="" type="checkbox"/> Antibodies
<input checked="" type="checkbox"/>	<input type="checkbox"/> Eukaryotic cell lines
<input checked="" type="checkbox"/>	<input type="checkbox"/> Palaeontology and archaeology
<input type="checkbox"/>	<input checked="" type="checkbox"/> Animals and other organisms
<input checked="" type="checkbox"/>	<input type="checkbox"/> Human research participants
<input checked="" type="checkbox"/>	<input type="checkbox"/> Clinical data
<input checked="" type="checkbox"/>	<input type="checkbox"/> Dual use research of concern

Methods

n/a	Involved in the study
<input checked="" type="checkbox"/>	<input type="checkbox"/> ChIP-seq
<input type="checkbox"/>	<input checked="" type="checkbox"/> Flow cytometry
<input checked="" type="checkbox"/>	<input type="checkbox"/> MRI-based neuroimaging

Antibodies

Antibodies used

For CyTOF, all antibodies were ordered from Fluidigm. Batch numbers are listed in order by order date (2018, 2019a, 2019b, 2020):
 Rat IgG2b Anti-Mouse CD45 (clone 30-F11) labelled with 89Y; catalog # 3089005B/C; batch # 0581829, 0161909, 0161909, 0622022
 Rat IgG2a Anti-Mouse Ly-6G (clone 1A8) labelled with 141Pr; catalog # 3141008B/C; batch # 2751702, 1201823, 1401910, 0132018
 Rat IgG2a Anti-MouseCD45R/B220 (clone RA3-6B2) labelled with 144Nd; catalog # 3144011B/C; batch # 2851711, 2851711, 2851711, 2851711
 Hamster IgG Anti-Mouse CD69 (clone H1.2F3) labelled with 145Nd; catalog # 3145005B/C; batch # 3511606, 3121831, 2211909, 1322039
 Rat IgG2a Anti-Mouse F4/80 (clone BM8) labelled with 146Nd; catalog # 3146008B/C; batch # 3121701, 0211903, 1901904, 2601904
 Rat IgG2b Anti-Mouse CD11b (Mac-1) (clone M1/70) labelled with 148Nd; catalog # 3148003B/C; batch # 3171702, 1401907, 1401907, 1401907
 Rat IgG2a Anti-Mouse CD19 (clone 6D5) labelled with 149Sm; catalog # 3149002B/C; batch # 0761711, 581828, 1901905, 1901905
 Rat IgG2b Anti-Mouse CD25 (IL-2R) (clone 3C7) labelled with 150Nd; catalog # 3150002B/C; batch # 1171712, 081811, 1981902, 3401917
 Rat IgG2a Anti-Mouse IgM (clone RMM-1) labelled with 151Eu; catalog # 3151006B/C; batch # 3001411, 1171710, 2681906, 2681906
 Hamster IgG Anti-Mouse CD3e (clone 145-2C11) labelled with 152Sm; catalog # 3152004B/C; batch # 3181714, 2971806, 2971806, 0132008
 Rat IgG2a Anti-Mouse CD8a (clone 53-6.7) labelled with 153Eu; catalog # 3168003B/C; batch # 1151403, 0101806, 2531901, 2531901
 Rat IgG2a Anti-Mouse Foxp3 (clone FJK-16s) labelled with 158Gd; catalog # 3158003A/C; batch # 3461707, 1841813, 2421903, 2421903
 IgG1 Anti-Mouse RORgt (clone B2D) labelled with 159Tb; catalog # 3159019B/C; batch # 3181709, 3181709, 3181709, 0912006
 Rat IgG2a Anti-Mouse CD5 (clone 53-7.3) labelled with 160Gd; catalog # 3160002B/C; batch # 2791503, 2791503, 2931525, 2791503
 IgG1 Anti-Mouse Tbet (clone 4B10) labelled with 161Dy; catalog # 3161014B/C; batch # 3391715, 3391715, 3181901, 3181901
 Rat IgG2c Anti-Mouse Ly-6C (clone HK1.4) labelled with 162Dy; catalog # 3162014B/C; batch # 2341706, 1201817, 2461904, 3431915
 Rat IgG2a Anti-Mouse CD62L (clone MEL-14) labelled with 164Dy; catalog # 3164003B/C; batch # 2851703, 2851703, 2691906, 2691906
 Rat IgG2a Anti-Mouse CD326 (EpCAM) (clone G8.8) labelled with 166Er; catalog # 3166014B/C; batch # 0251601, 0251601, 0251601, 0251601
 Rat IgG2b Anti-Mouse Gata3 (clone TWAJ) labelled with 167Er; catalog # 3167007A/C; batch # 3481606, 0391808, 2551902, 0592011
 Rat IgG2a Anti-MouseCD206 (MMR) (clone C068C2) labelled with 169Tm; catalog # 3169021B/C; batch # 0711816, 1341903, 2671901, 0282009
 Hamster IgG Anti-Mouse CD49b (clone HMa2) labelled with 170Er; catalog # 3170008B/C; batch # 2851710, 3511803, 3511803, 3511803
 Rat IgG2b Anti-Mouse CD44 (clone IM7) labelled with 171Yb; catalog # 3171003B/C; batch # 1931725, 1201828, 2461903, 3181915
 Rat IgG2a Anti-Mouse CD4 (clone RM4-5) labelled with 172Yb; catalog # 3172003B/C; batch # 1201808, 3391809, 3391809, 3391809
 Rat IgG2b Anti-Mouse CD117 (ckit) (clone 2B8) labelled with 173Yb; catalog # 3173004B/C; batch # 0331524, 2631811, 2631811, 0452003
 Rat IgG2b Anti-Mouse I-A/I-E (MHC Class II) (clone M5/114.15.2) labelled with 174Yb; catalog # 3174003B/C; batch # 0791514, 2631807, 2631807, 2631807
 Rat IgG2a Anti-Mouse CD38 (clone 90) labelled with 175Lu; catalog # 3175014B/C; batch # 0341403, 2041807, 2041807, 2041807
 Hamster IgG Anti-Mouse FceR1a (clone 36951) labelled with 176Yb; catalog # 3176006B/C; batch # 2381302, 0381905, 0381905, 0381905
 Hamster IgG Anti-Mouse CD11c (clone N418) labelled with 209Bi; catalog # 3209005B/C; batch # 0081812, 1521804, 1521804, 2007297-27

The following antibodies were used for flow cytometry:

Rat IgG2a kappa Anti-Mouse CD4 (clone RM4-5) labelled with BV605, Biolegend (catalog #100548; lot #B279163 – July 2019)
 Rat IgG2a kappa Anti-Mouse CD45R/B220 (clone RA3-6B2) labelled with BV650, BD Horizon™/BD Biosciences (catalog #563893; lot #8332815 – May 2019, #0195860 – Sept & Dec 2020)
 Rat IgG2b kappa Anti-Mouse CD3 (clone 17A2) labelled with BV711, Biolegend (catalog #100241; lot #B245637 – Nov 2018, #B265870 – Apr 2019, #B330904 – Apr & Jun 2021)
 Rat IgG2b kappa Anti-Mouse CD45 (clone 30-F11) labelled with BV786, BD Horizon™/BD Biosciences (catalog #564225; lot #9311117 – Jun 2020, #0177317 – Dec 2020, #1063428 – Jun 2021, # 1175935 – Oct 2021)
 Rat IgG2a kappa Anti-Mouse CD8 (clone 53-6.7) labelled with PE-Cy5, Biolegend (catalog #100710, lot #B300603 – Jun 2020)
 Rat IgG2a kappa Anti-Mouse IL-17A (clone eBio17B7) labelled with eFluor506, eBioscience™ (catalog #69-7177-82; lot #2029236 – Jul

2019)
 Rat IgG1 kappa Anti-Mouse IL-13 (clone eBio13A) labelled with Alexa Fluor 488, eBioscience™ (catalog #53-7133-82; lot #2211046 – Aug 2020)
 Rat IgG1 kappa Anti-Mouse TNF alpha (clone MP6-XT22) labelled with PerCP-eFluor710, eBioscience™ (catalog #46-7321-82; lot #1998358 – Jun 2019)
 Rat IgG1 kappa Anti-Mouse/Anti-Human IL-5 (clone TRFK5) labelled with PE, BD Pharmingen™/BD Biosciences (catalog #554395; lot #8130811 – Jul 2020)
 Rat IgG1 kappa Anti-Mouse IFN gamma (clone XMG1.2) labelled with PE-eFluor610, eBioscience™ (catalog #61-7311-82; lot #2071327 – Jul 2019)
 Rat IgG2b kappa Anti-Mouse CD45 (clone30-F11) labelled with PE-Cy7, BD Pharmingen™/BD Biosciences (catalog #552848; lot #8205729 – Apr 2019, #9352096 – Feb 2020)
 Rat IgG2a kappa Anti-Mouse Siglec-F (clone E50-2440) labelled with BV786, BD OptiBuild™/BD Biosciences (catalog #740956; lot #226552 – Aug 2020, #1116710 – May 2021)
 Rat IgG2b kappa Anti-Mouse CD11b (clone M1/70) labelled with PE-CF594, BD Horizon™/BD Biosciences (catalog #562287; lot #188007 – Oct 2020)

The following antibody was used to stain the mucus:

Rabbit monoclonal anti-MUC2 antibody (clone EPR23479-47, catalog #. ab272692, Abcam, Amsterdam, Netherlands)

The following antibodies were used for ELISA:

Mouse Anti-Ovalbumin IgE (Clone E-C1, catalog #. 7091, Ams Biotechnology, Abingdon, UK)
 Mouse anti-ovalbumin IgG1 (Clone L71, catalog #. 7093, Ams Biotechnology, Abingdon, UK)
 Phosphatase alkaline-conjugated goat anti-mouse IgE (SouthernBiotech, catalog #. 1110-04, ImTec Diagnostics, Antwerp, Belgium)
 Phosphatase alkaline-conjugated goat anti-mouse IgG1 (SouthernBiotech, catalog #. 1071-04, ImTec Diagnostics, Antwerp, Belgium)
 Rat anti-mouse IgE (SouthernBiotech, catalog #. 1130-01, ImTec Diagnostics, Antwerp, Belgium)
 Rat anti-mouse IgG1 (SouthernBiotech, catalog #. 1144-01, ImTec Diagnostics, Antwerp, Belgium)

Validation

Standard, commercially available antibodies and their metal tags were selected in consultation with specialists from Fluidigm and validated on test samples prior to their application in this study. Both fluorescent- and metal-tagged antibodies were titrated according to the manufacturer's recommendation in preliminary experiments in order to determine appropriate concentration.

Animals and other organisms

Policy information about [studies involving animals](#); [ARRIVE guidelines](#) recommended for reporting animal research

Laboratory animals

The study involved 6-10 week-old, female Balb/c mice.

Wild animals

The study did not involve wild animals.

Field-collected samples

The study did not involve samples collected from the field.

Ethics oversight

All specific-pathogen-free (SPF) animal experiment protocols were approved by the Animal Welfare Service at the Luxembourg Institute of Health, and further approved by the Veterinary Services Administration within the Ministry of Agriculture (national authorization no. LUPA2018/18, LUPA2019/29). All germ-free (GF) and gnotobiotic animal experiment protocols were approved by the Animal Experimentation Ethics Committee (AEEC) at the University of Luxembourg (national authorization no. LUPA2019/50). Mice were housed in individually ventilated cages (Techniplast Sealsafe Plus GM500 or Allentown Sentry SPP™ Mouse cages in SPF or GF/gnotobiotic facilities, respectively) at 20-24°C with 40-70% humidity, under 12-hour light cycles. Sterile water and diets were provided ad libitum.

Note that full information on the approval of the study protocol must also be provided in the manuscript.

Flow Cytometry

Plots

Confirm that:

- The axis labels state the marker and fluorochrome used (e.g. CD4-FITC).
- The axis scales are clearly visible. Include numbers along axes only for bottom left plot of group (a 'group' is an analysis of identical markers).
- All plots are contour plots with outliers or pseudocolor plots.
- A numerical value for number of cells or percentage (with statistics) is provided.

Methodology

Sample preparation

Isolated cells were washed with PBS and incubated with Zombie NIR (Catalogue no. 423105, Biolegend Europe BV, Amsterdam, Netherlands), for 15 min at 4°C, prior to fixation with the Cytofix/Cytoperm solution kit (BD Biosciences, Erembodegem-Aalst, Belgium). Cells were then washed with FACS buffer, incubated with Fc block (1 µg/million cells, catalogue no. 553142, BD Biosciences, Erembodegem-Aalst, Belgium) for 15 min and stained with the antibody mix (Extended data Table 1) for 30 min at 4°C. Samples were finally washed and resuspended in PBS for acquisition.

Instrument

NovoCyte Quanteon Flow Cytometer (ACEA Biosciences).

Software	FCS files were analyzed in FlowJo™ (BD Biosciences)
Cell population abundance	At least 200 000 events were acquired.
Gating strategy	For each reported population, counts were normalized to the LD-CD45+/Single Cells/Width, SSC-H subset and results are presented as a percentage of CD45+ cells.

Tick this box to confirm that a figure exemplifying the gating strategy is provided in the Supplementary Information.